PHYSICAL REVIEW D **90,** 063501 (2014)

Compatibility of Planck and BICEP2 results in light of inflation

Jérôme Martin,[1,*] Christophe Ringeval,[2,†] Roberto Trotta,[3,‡] and Vincent Vennin[1,§]

[1]*Institut d'Astrophysique de Paris, UMR 7095-CNRS, Université Pierre et Marie Curie, 98 bis boulevard Arago, 75014 Paris, France*

[2]*Centre for Cosmology, Particle Physics and Phenomenology, Institute of Mathematics and Physics, Louvain University, 2 Chemin du Cyclotron, 1348 Louvain-la-Neuve, Belgium*

[3]*Imperial College London, Astrophysics & Imperial Centre for Inference and Cosmology, Blackett Laboratory, Prince Consort Road, London SW7 2AZ, United Kingdom*

(Received 3 June 2014; published 2 September 2014)

We investigate the implications for inflation of the detection of *B*-modes polarization in the cosmic microwave background by BICEP2. We show that the hypothesis of the primordial origin of the measurement is favored only by the first four band powers, while the others would prefer unreasonably large values of the tensor-to-scalar ratio. Using only those four band powers, we carry out a complete analysis in the cosmological and inflationary slow-roll parameter space using the BICEP2 polarization measurements *alone* and extract the Bayesian evidences and complexities for all the *Encyclopædia Inflationaris* models. This allows us to determine the most probable and simplest BICEP2 inflationary scenarios. Although this list contains the simplest monomial potentials, it also includes many other scenarios, suggesting that focusing model building efforts on large field models only is unjustified at this stage. We demonstrate that the sets of inflationary models preferred by Planck alone and BICEP2 alone are almost disjoint, indicating a clear tension between the two data sets. We address this tension with a Bayesian measure of compatibility between BICEP2 and Planck. We find that for models favored by Planck the two data sets tend to be incompatible, whereas there is moderate evidence of compatibility for the BICEP2 preferred models. As a result, it would be premature to draw any conclusion on the best Planck models, such as Starobinsky and/or Kähler moduli inflation. For the subset of scenarios not exhibiting data sets incompatibility, we update the evidences and complexities using both data sets together.

DOI: 10.1103/PhysRevD.90.063501 PACS numbers: 98.80.Cq

I. INTRODUCTION

The recent discovery of *B*-mode polarization in the Cosmic Microwave Background (CMB) by BICEP2 [1], if confirmed to be of primordial origin [2], would constitute a breakthrough for our understanding of early universe cosmology. In addition to lensing, *B* mode can be generated by either vector perturbations or tensor perturbations [3]. Vectors do not propagate in a Friedmann-Lemaître universe (see, however, Ref. [4]) and can be a potential explanation of the BICEP2 data only if they are incessantly generated by active sources such as cosmic strings [5–7] or magnetic fields [8]. These, however, are severely constrained by other measurements [9,10].

Tensor modes are a natural and expected outcome of cosmic inflation although the uncertainty on their amplitude is huge (several orders of magnitude). In this context, the BICEP2 result might represent the first detection of primordial gravity waves produced in the early universe [11,12] and, therefore, could give us precious information about the physical conditions that prevailed at that time. Of course, the BICEP2 result needs to be confirmed by other measurements before one can be sure that primordial *B*-modes have really been detected. In this paper, our working hypothesis will be that this is indeed the case. On general grounds, it is anyway always interesting to explore the implications for inflation of a non-negligible level of primordial gravity waves.

The claimed amplitude of the signal corresponds to a tensor-to-scalar ratio of $r = 0.2^{+0.07}_{-0.05}$ or $r = 0.16^{+0.06}_{-0.05}$ depending on how polarized dust foregrounds are modeled and/or subtracted. Recent works [13] have, however, cast doubts on the modeling of the foreground dust, which could potentially lead to the amplitude of the tensor modes signal to be much lower, to the point of becoming undetectable. In the following, we shall take the BICEP2 result at face value, pending further investigation, most notably thanks to the recently released Planck dust maps [14]. The BICEP2 measurement, if, as already mentioned, interpreted as of primordial origin, has several important physical consequences that we now discuss.

First, the energy scale of inflation [15–24] is fixed and roughly given by

$$\rho^{1/4} \simeq 2.2\left(\frac{r}{0.2}\right)^{1/4} 10^{16}\ \text{GeV}, \tag{1}$$

*jmartin@iap.fr
†christophe.ringeval@uclouvain.be
‡r.trotta@imperial.ac.uk
§vennin@iap.fr

i.e. around the grand unified theory (GUT) energy scale. A more accurate determination of this energy scale and the Hubble rate during inflation are given in Sec. III D. Inflation is therefore a high energy phenomenon by particle physics standard.

Second, this result would favor that single field slow-roll scenarios achieve the best compromise between quality of the fit and theoretical simplicity [25]. Indeed, in more complicated models, the tensor-to-scalar ratio is generically (but not necessarily) smaller than in the standard case.[1] For instance, for K inflation [28], one has $r = -8n_{\mathrm{T}}c_{\mathrm{s}}$ where $c_{\mathrm{s}} < 1$ is the sound speed of the fluctuations [29]. For two-field inflation, one can write $r = -8n_{\mathrm{T}}\sin^2\Theta \leq -8n_{\mathrm{T}}$, where $\sin\Theta$ is a term taking into account the possible evolution of scalar modes on super Hubble scales [30]. For multiple field inflation, the above equality becomes an inequality, namely $r \leq -8n_{\mathrm{T}}\sin^2\Theta$, thus strengthening the argument presented before (up to the special case of massive Nflation which inherits some of the properties of a single $m^2\phi^2$ model [31–34]). Of course, this certainly does not mean that these more complicated models are ruled out by BICEP2 (as a matter of fact, they are not), but together with the absence of detection of isocurvature modes and primordial non-Gaussianities, this reinforces the fact that they are not needed in order to give a satisfactory description of the data. Clearly, this argument should be toned down given that multiple field models are often well motivated from a high energy point of view and, moreover, can predict a non-negligible r even if the field excursion is smaller than the Planck mass [35] (see below). Also notice that, for the simplest and preferred class of inflationary models mentioned above, the non-Gaussianities are characterized by $f_{\mathrm{NL}}^{\mathrm{loc}} = 5(1-n_{\mathrm{S}})/12 \simeq 1.6\times10^{-2}$ [36] since Planck [37,38] has measured $n_{\mathrm{S}} = 0.9603 \pm 0.0073$. Therefore, unless one is able to reach the 10^{-2} level, it seems impossible to measure $V(\phi)$ using the precise shape of the three-point correlation function. The 10^{-2} level appears to be extremely challenging given our present day capabilities and, as a consequence, this reinforces the importance of a measurement of r since this opens a realistic opportunity to identify the correct inflationary scenario.

Third, in the framework of single field slow-roll scenarios, the BICEP2 result implies a lower bound on the first Hubble flow function, which is also given by $\epsilon_1 \simeq M_{\mathrm{Pl}}^2(V_\phi/V)^2/2$. Therefore, the first derivative of the inflaton potential can be constrained. Furthermore, since the deviation from scale invariance $n_{\mathrm{S}}-1$ depends on a combination of the first and second derivatives of the potential (at leading order in slow roll), this automatically also provides a measurement of the second derivative of the potential. It is also interesting to notice that a constraint on ϵ_1 does not modify our estimate of the importance of the stochastic effects for CMB scales [39–41]. Indeed, if Δ_{q} is the typical quantum excursion of the inflaton field during one e-fold and Δ_{cl} its classical excursion, then $\Delta_{\mathrm{q}}/\Delta_{\mathrm{cl}} \simeq H/(M_{\mathrm{Pl}}\sqrt{\epsilon_1}) \simeq \sqrt{\mathcal{P}_\zeta} \simeq 10^{-5}$. The point is that $\Delta_{\mathrm{q}}/\Delta_{\mathrm{cl}}$ does not depend on ϵ_1 alone but on the combination $H/\sqrt{\epsilon_1}$ which was already measured before BICEP2 since it turns out to be exactly the amplitude of the scalar modes. However, a measurement of r also gives indications about the shape of the potential (see below) and, then, $\Delta_{\mathrm{q}}/\Delta_{\mathrm{cl}} > 1$ may become possible but necessarily outside the observable window. If $r \simeq 0.2$ favors potentials for which this systematically happens, one should still pay attention to how measurements made on the CMB scales should be extrapolated to the part of the inflaton's potential supporting a stochastic regime [42]. Therefore, observationally speaking, the question of knowing if nonperturbative quantum effects can play an important role in the early universe is still open [43–45].

Fourth, the model building problem is also impacted by the BICEP2 result. Indeed, by definition of the first Hubble flow function, one has $\Delta\phi/M_{\mathrm{Pl}} = \mathcal{O}(1)(r/0.2)^{1/2}$ [46,47] which indicates that the excursion of the field during inflation is necessarily super-Planckian. The single field models discussed before are usually viewed as effective models only, valid up to a cutoff Λ [48]. This scale should be less than M_{Pl} since M_{Pl} is the cutoff of general relativity and larger than H since the model should be able to describe what happens during inflation. In the framework of effective field theories, when physical effects beyond the cutoff are taken into account, the total Lagrangian of a given inflationary model can be expressed as $\mathcal{L} = \dot\phi^2/2 + V(\phi) + \sum_i c_i\mathcal{O}_i/\Lambda^{n_i-4}$, where $V(\phi)$ contains renormalizable terms only and $\mathcal{O}_i$ represents a higher order operator of dimension $n_i > 4$ (possibly a nonminimal kinetic term) the amplitude of which is controlled by the coefficient c_i. When an inflationary model is designed, it usually makes use of $\mathcal{L} = \dot\phi^2/2 + V(\phi)$ only and the higher order operators are neglected. The validity of this approximation is questionable because of the following two problems. First, as mentioned above, a large value of r implies a large value of $\Delta\phi$ compared to the Planck mass and the operators $\mathcal{O}_i$ may no longer be negligible. Solutions to these issues are either to fine-tune the couplings between the light and heavy fields or to assume the existence of a symmetry (typically the shift symmetry) to forbid the dangerous higher order operators. But, then, this raises the question of the origin of this symmetry in the full theory, that is to say the question of the UV completion of the model. For a nice and more complete discussion on all these issues, see for instance Ref. [48]. Second, the parameters of $V(\phi)$ usually get corrected by heavy field loops. For instance, a mass term typically acquires the following form: $m^2 \to m^2 + gM^2\ln(\Lambda/\mu)$, where μ is a

[1]With the notable exception of G inflation [26,27] where $r = 16c_{\mathrm{s}}\sigma$, with σ a complicated function of the inflaton field and its derivative, possibly larger than 1 even in the slow-roll limit.

renormalizable scale, $M > \Lambda$ the mass of a heavy field and g the coupling between ϕ and the heavy field.[2] This means that the mass of the inflaton becomes larger than the Hubble rate and that the potential is no longer flat enough to support inflation. Notice, however, that this issue is, *a priori*, always present even in a model where r is small.

Fifth, the BICEP2 result exacerbates the problems of inflationary magnetogenesis [50–52]. Recent observations indicate the presence of magnetic fields of strength ranging from 10^{-17} to 10^{-15} Gauss on megaparsec scales and such a large coherence length suggests a cosmological origin [53–56]. In order to produce a magnetic field during inflation, one needs to break conformal invariance. For instance, this can be achieved by considering a term $f^2(\phi)F_{\mu\nu}F^{\mu\nu}$. A simple parametrization for the function $f(\eta)$ is given by $f \propto a^\alpha$ [52] since the choices $\alpha \simeq 2$ or $\alpha \simeq -3$ both lead to a flat spectrum. For $\alpha = 2$ f is a growing function of time, and since the gauge field A_μ is also coupled to charged fermions with a coupling constant $g_{\rm eff}(\eta) \propto g/f(\eta)$, this implies that the system is in a nonperturbative regime during inflation [57] (for a possible solution, see Refs. [58,59]). On the other hand, the solution $\alpha = -3$ suffers from a backreaction problem. In order to avoid a too important production of the electric field, the only way out is then to lower the energy scale of inflation, i.e. $H/M_{\rm Pl} \lesssim 10^{-20}$ [52,60,61]. The BICEP2 result would invalidate this solution and, therefore, one is left in a situation where inflationary magnetogenesis appears to be more problematic than before.

Sixth, the detection of a quite large value of r raises the question of whether one can directly see the primordial gravitational waves. With $r \simeq 0.2$ and $n_{\rm T} \simeq -r/8 \simeq -0.025$ [see Eq. (28)], one expects to have today $\Omega_{\rm gw} \simeq 10^{-15}$ and experiments such as VIRGO [62] and eLISA [63] cannot detect such a tiny signal. However, Japan's DECIGO [64,65], Ultimate-DECIGO or NASA's Big Bang Observer [66] have *a priori* the sensitivity required to directly probe the inflationary primordial gravity waves. Notice that these experiments operate in the frequency range $f \in [10^{-2}\ {\rm Hz}, 10\ {\rm Hz}]$ and this could render the measurements of the reheating parameters, such as the reheating temperature and/or the equation of state parameter, feasible [67,68].

[2]Notice that regularizing the loop integral with a cutoff would have produced a correction proportional to Λ^2, namely $m^2 \to m^2 + g\Lambda^2$. However, this approach is not consistent as can be nicely illustrated on the example of the regularization of the cosmological constant. Indeed, if one regularizes $\rho_{\rm vac}$ with a cutoff, one obtains that $\rho_{\rm vac} \to \rho_{\rm vac} + \Lambda^4$. However, this method breaks Lorentz invariance and, as a consequence, one obtains the wrong equation of state, $w = p_{\rm vac}/\rho_{\rm vac} = 1/3$ instead of $w = -1$. If, on the contrary, the loop integral is regularized with a method that respects Lorentz invariance (for instance dimensional regularization), then one obtains $\rho_{\rm vac} \to \rho_{\rm vac} + M^4 \ln(\Lambda/\mu)$ and $w = -1$; see Ref. [49]. In other words, if there is no new physics beyond the standard model, there is no hierarchy problem.

Seventh, it has been claimed [69–71] that the BICEP2 results would represent the first experimental evidence for quantum gravity since, in the framework of inflation, the transverse and traceless component of the perturbed metric is a quantum operator. This has indeed been known for 40 years [11,12] and more than 20 years in the context of inflation [72–74]. However, this was already the case for scalar modes [23,72–74]. Indeed, their equation of motion derives from the perturbed quantum Einstein equations, $\delta\hat{G}_{\mu\nu} = 8\pi G\delta\hat{T}_{\mu\nu}$. To put it differently, the Mukhanov-Sasaki quantum operator $\hat{v}$, which characterizes the amplitude of scalar modes, is expressed in terms of the perturbed inflaton field $\delta\hat{\phi}$ and the Bardeen potential $\hat{\Phi}$, concretely $\hat{v} \equiv \delta\hat{\phi} + (\phi'/\mathcal{H})\hat{\psi} = \delta\hat{\phi}^{\rm (gi)} + (\phi'/\mathcal{H})\hat{\Phi}$ (where $\delta\hat{\phi}^{\rm (gi)}$ is the gauge invariant perturbed field and $\hat{\psi}$ is the scalar component of the perturbed metric proportional to δ_{ij}). We see that the perturbed metric is also a quantum operator in the scalar sector and is directly related to the CMB anisotropies. Notice that a semiclassical formulation of the problem, namely $\delta G_{\mu\nu} = 8\pi G\langle\delta\hat{T}_{\mu\nu}\rangle$, does not help since $\delta\hat{T}_{\mu\nu}$, being by definition linear in $\delta\hat{\phi}$, satisfies $\langle\delta\hat{T}_{\mu\nu}\rangle = 0$. One might argue that the scalar sector suffers from a gauge problem but this question has been discussed and solved with the help of the gauge-invariant formalism [75]. There exists a gauge (the spatially flat or uniform curvature gauge [76]) for which $\psi = 0$ and, therefore, $v = \delta\phi$. However, this cannot be used as an argument that only field fluctuations must be quantized. Indeed, there is another gauge (comoving orthogonal gauge [76]) where $\delta\phi = 0$ and, hence, $v = (\phi'/\mathcal{H})\psi$. As a consequence, the same logic leading to the above argument could also be used to reach an opposite conclusion, namely that only metric fluctuations (and not field perturbations) must be quantized. In fact, as it is clear from the definition of the Mukhanov-Sasaki variable, field and metric perturbations cannot be disentangled [77] and the scalar modes are therefore already a genuine signature of the quantum-mechanical nature of the gravitational field. On the other hand, it is true that there still exist open issues related to the quantum to classical transition of these quantum fluctuations [78–86].

Eighth, it is worth recalling that BICEP2 data do not only concern the B-mode polarization but also the E modes ($C_\ell^{\rm TT,obs}$ and $C_\ell^{\rm TE,obs}$ are not yet publicly available). The fact that the polarization spectrum $C_\ell^{\rm EE,obs}$ has also been measured is fortunate since it allows us to constrain scalar perturbations, and cosmology, with the BICEP2 data alone [87]. This is discussed further in the following. Although not public, the BICEP2 team reports a $C_\ell^{\rm TB,obs}$ consistent with zero, and this is relevant for models containing a gravitational Chern-Simons term [88–90]. This term is necessarily present since it is generated by quantum corrections and is generic in string theory. This implies that the two polarization states of a gravitational wave

behave differently. As a consequence, the tensor-to-scalar ratio is modified and can even be enhanced [89] (to be fair, a calculation of r in a regime where the enhancement is large remains very challenging).

Another question which arises after BICEP2 is the implications of these new data with regards to the shape of the inflaton potential $V(\phi)$ and whether these implications are compatible with the conclusions reached previously, and notably from Planck data [25,91–93]. Let us recall that, given Planck data, the best models in terms of evidences and complexities are such that their potential is of the plateau type, the prototypical example being the Starobinsky model [15]. In more quantitative terms, if one uses the Jeffreys scale [94,95] and counts the number of models in the "inconclusive," "weak evidence," "moderate evidence," and "strong evidence" zones with respect to the best, one finds 26% in the first category (corresponding to 17 different shapes of the potential), 21% in the second, 17% in the third, and, finally, 34% in the fourth and last one. These numbers can be further improved by another statistical indicator. If we restrict ourselves to models having a number of unconstrained parameters between 0 and 1, then only 9% of the scenarios are preferred, corresponding this time to 9 different potentials. And these 9 potentials are all of the plateau type. On the other hand, the Jeffreys scale has to be taken as indicative, and it is usually considered that only the models belonging to the strong evidence category (here, 34%) can really be considered as robustly "ruled out." Therefore, we see that the Planck data have been able to narrow down our theoretical uncertainties efficiently and to point to a particular type of potentials. As a consequence, an important question is whether the BICEP2 measurements are in agreement with these conclusions and, more generally, whether BICEP2 is compatible with Planck in the framework of single field slow-roll inflation.

The present article aims at discussing the issues presented above. As many inflationary models genuinely produce a small amount of tensor modes, one would expect the BICEP2 data to severely cut a large volume of the model space, thereby improving our knowledge of inflation compared to what has already been established with Planck data. However, one has first to address and quantify the compatibility between BICEP2 and Planck data. For this, it is required to first investigate both data sets independently. This may seem problematic for BICEP2 as B modes alone do not give constraints on the scalar perturbations. But, as we show below, using both the E and B modes polarization measurements in only four band powers already gives nontrivial constraints on both the standard cosmological parameters and the primordial ones (see also Ref. [87]). This allows us to derive the evidences and complexities of all the *Encyclopædia Inflationaris* models using BICEP2 data alone and thoroughly discuss the compatibility of Planck and BICEP2 using the so-called $\mathcal{R}$ factors [96–102]. These are the Bayes factors giving the ratio between the probability of compatibility to the probability of incompatibility assuming a given model. By evaluating $\mathcal{R}$ for slow-roll inflation and for each *Encyclopædia Inflationaris* scenarios, one can determine the subset of models for which Planck and BICEP2 data can be meaningfully combined to obtain evidences and complexities from the joint data sets.

This article is organized as follows. In the next section, we briefly describe the method used to compute the Bayesian evidence of any slow-roll inflationary model. In particular, our method is based on the determination of an effective likelihood for inflation which requires a slow-roll analysis of the Planck and BICEP2 data. The results of the analysis for Planck can be found in Ref. [25], and we present in Sec. III new results for BICEP2 alone and BICEP2 combined with Planck. In particular, we discuss the compatibility of the data sets under the hypothesis of slow roll. In Sec. IV, we present the evidences and complexities for all the *Encyclopædia Inflationaris* models stemming from the BICEP2 data alone and discuss what are the inflaton potential shapes favored and how they differ from the Planck results. We then move on to the compatibility of Planck and BICEP2 model by model and present joint evidences and complexities for the scenarios under which both data sets are not incompatible. Finally, in Sec. V, we summarize our findings and present our conclusions.

II. METHODOLOGY

A. Bayesian evidence and complexity

In this section, we briefly present the statistical methodology adopted here to compute the Bayesian evidence and complexity for each of the *Encyclopædia Inflationaris* models that, in the following, we denote by $\mathcal{M}_i$.

The Bayesian evidence, given data D, is defined by [95]

$$P(D|\mathcal{M}_i) \equiv \mathcal{E}(D|\mathcal{M}_i) = \int \mathrm{d}\theta_{ij}\mathcal{L}(\theta_{ij})\pi(\theta_{ij}|\mathcal{M}_i), \quad (2)$$

where θ_{ij} represents the parameters characterizing the model $\mathcal{M}_i$, $\mathcal{L}$ is the likelihood function (to be discussed below), and $\pi(\theta_{ij}|\mathcal{M}_i)$ is the prior distribution for the parameter θ_{ij}. As usual in Bayesian analysis, the choice of the priors plays a crucial role, and a complete study of the $\pi(\theta_{ij}|\mathcal{M}_i)$ for all the *Encyclopædia Inflationaris* models can be found in Ref. [25]. Here, we adopt the same choices. The Bayesian complexity can be expressed as [103]

$$\mathcal{C}_i = \langle -2\log\mathcal{L}(\theta_{ij})\rangle + 2\log\mathcal{L}(\theta_{ij}^{\mathrm{ML}}), \quad (3)$$

where $\langle\cdot\rangle$ means averaging over the posteriors and $\theta_{ij}^{\mathrm{ML}}$ represents the maximum likelihood estimate of the model's parameters.

The Bayesian evidences are often normalized to a reference model $\mathcal{M}_{\rm REF}$, and one defines $B^i_{\rm REF} \equiv \mathcal{E}(D|\mathcal{M}_i)/\mathcal{E}(D|\mathcal{M}_{\rm REF})$. They give us information about the posterior probability of the model $\mathcal{M}_i$ (for noncommittal model priors),

$$P(\mathcal{M}_i|D) = \frac{B^i_{\rm REF}}{\sum_j B^j_{\rm REF}}. \tag{4}$$

On the other hand, the Bayesian complexities tell us something about the number of unconstrained parameters

$$N^{\rm uc}_i \equiv N_i - \mathcal{C}_i, \tag{5}$$

where N_i is the total number of parameters of the model under scrutiny. The above considerations show that, given a data set D, the performance of a model can be described by the numbers $(N^{\rm uc}, B_{\rm REF})$.

B. Compatibility of data sets

Although the previous discussion is readily applicable for either the Planck ($D_{\rm p}$) or BICEP2 data ($D_{\rm b}$) separately, computing a joint evidence from BICEP2 and Planck, namely using $D = \{D_{\rm p}, D_{\rm b}\}$, requires some precaution. Indeed, it is crucial to determine whether a small value of $P(D|\mathcal{M}_i)$ is the consequence of $\mathcal{M}_i$ being a poor explanation of the data, or whether this results from the tension between Planck and BICEP2.

As detailed below, there is a tension between the two data sets, when interpreted in terms of tensor modes amplitude. Combining the two data sets blindly could potentially lead to a joint likelihood function that peaks in a region of parameter space that is not favored by either experiment—an obviously undesirable situation.

In order to study the compatibility of BICEP2 and Planck, we resort to a Bayesian measure defined as follows [96–102,104]:

$$\mathcal{R}_i \equiv \frac{P(D_{\rm p}, D_{\rm b}|\mathcal{M}_i, \mathcal{H}_{\rm c})}{P(D_{\rm p}|\mathcal{M}_i, \mathcal{H}_{\rm ic}) P(D_{\rm b}|\mathcal{M}_i, \mathcal{H}_{\rm ic})}. \tag{6}$$

This quantity represents the posterior between the hypothesis that the two data sets are compatible ($\mathcal{H}_{\rm c}$, when $\mathcal{R}_i > 1$) versus the hypothesis that they are not ($\mathcal{H}_{\rm ic}$ and thus described by different sets of parameters, when $\mathcal{R}_i < 1$), assuming the inflationary model $\mathcal{M}_i$ and noncommittal priors between the two hypotheses, $P(\mathcal{H}_{\rm c}) = P(\mathcal{H}_{\rm ic}) = 1/2$. Various prototypical situations illustrating the behavior or $\mathcal{R}$ are presented in the Appendix (see Sec. A 1), where one can gain some insight on why $\mathcal{R}$ measures compatibility. The $\mathcal{R}$ factor can also be reexpressed in terms of the conditional predictive probability for BICEP2 data, by noting that

$$P(D_{\rm p}, D_{\rm b}|\mathcal{M}_i) = P(D_{\rm b}|D_{\rm p}, \mathcal{M}_i) P(D_{\rm p}|\mathcal{M}_i). \tag{7}$$

Using Eq. (7), we obtain the simpler expression

$$\mathcal{R}_i = \frac{P(D_{\rm b}|D_{\rm p}, \mathcal{M}_i)}{P(D_{\rm b}|\mathcal{M}_i)}, \tag{8}$$

which shows that $\mathcal{R}_i$ is large if the probability of obtaining data $D_{\rm b}$, given the Planck data $D_{\rm p}$, is large.

C. Likelihood functions

The likelihoods considered in the following have been provided by the Planck Collaboration [105] and the BICEP2 team [1,106,107]. Concerning the Planck likelihood, we have used the "CamSpec" likelihood for the temperature power spectrum in the multipole range $50 < \ell < 2500$ complemented with the "Commander" likelihood for $2 < \ell < 49$. Moreover, following the data analysis method of Refs. [37,108], we have also used the WMAP polarization data for $\ell \leq 32$ [109–111]. These data sets are the same as the ones used in Ref. [25]. Concerning the BICEP2 likelihood, we have written a FORTRAN code from scratch based on the approximation of Ref. [106] and as implemented by the BICEP2 team (see Ref. [112]). Our results are identical to the ones obtained with the latest version of COSMOMC [113] in which the BICEP2 likelihood has also been implemented. The BICEP2 measurements are publicly available.[3]

As discussed in Ref. [1], when assuming primordial power law power spectra, the BICEP2 likelihood for the tensor-to-scalar ratio r peaks at a value around 0.2, which is significantly larger than those favored by the Planck data. In Figs. 1 and 2, we have represented the BICEP2 likelihood profile along r, in each band power, when the ΛCDM cosmological parameters are fixed to their mean values obtained from the Planck data alone [37]. Let us notice that the likelihood has been estimated using CAMB [114] to provide the expected $C_\ell^{\rm BB,th}$ for each value of r while including the lensing effects which convert E modes into B modes. This figure shows that over the nine band powers provided by the BICEP2 team, the second bin carries most of the statistical weight and, moreover, only four bins are reasonable with the hypothesis that the measured $C_\ell^{\rm BB,obs}$ are sourced by tensor modes of inflationary origin. Indeed, already for the band power five, the likelihood peaks at a value $r > 0.5$. The band powers six to nine would even favor a tensor-to-scalar ratio larger than 1. Those band powers do not significantly weigh in the total likelihood as their associated errors are relatively large (see Fig. 1). However, as they seem to suffer from a systematic excess, the origin of which not being inflation or lensing, we have decided to perform our data analysis using only the first four band powers of the BICEP2 data hoping that they are not too much affected by such systematics. In fact, we

[3]See http://bicepkeck.org.

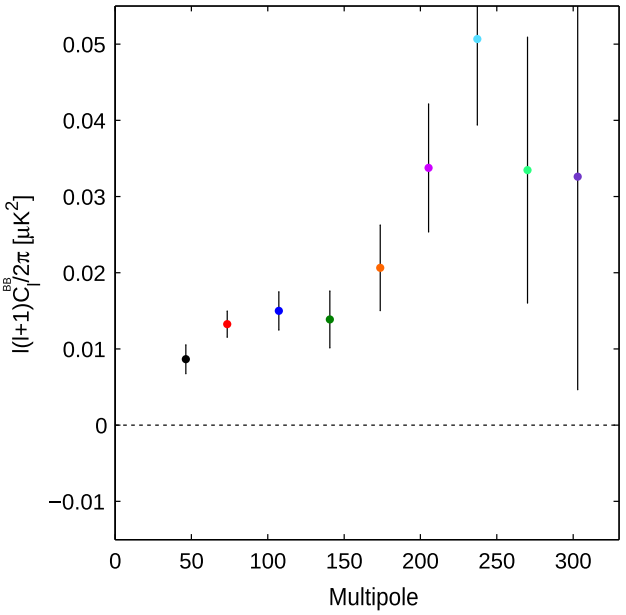

FIG. 1 (color online). *B*-mode angular power spectrum in the nine band powers measured by the BICEP2 experiment. Figure extracted from Ref. [1].

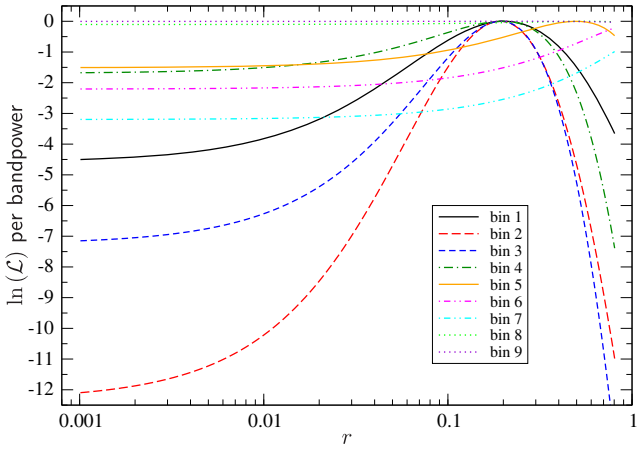

FIG. 2 (color online). BICEP2 likelihood function over the tensor-to-scalar ratio r, assuming power law primordial spectra and with the ΛCDM parameters fixed to their mean value obtained from the Planck data alone. *B* modes from lensing are included, and we have presented the contribution of each of the nine BICEP2 band powers. Only the first four band powers favor the hypothesis of primordial tensor modes of inflationary origin, whereas the others exhibit a likelihood maximal at problematic large values of r.

have also checked that including all the bins in the analysis does not modify in a substantial way our conclusions.

D. Fast evidence computation

Given our likelihood function, we briefly summarize in this section how the Bayesian evidence of a given *Encyclopædia Inflationaris* model can be fast computed.

Any inflationary model is characterized by the parameters $\theta_{\rm inf}$ describing the shape of the potential [for instance, for large field inflation where $V(\phi) = M^4(\phi/M_{\rm Pl})^p$, one has $\theta_{\rm inf} = (M, p)$] and by the priors' choice on those parameters [25]. We also need parameters describing the reheating phase, $\theta_{\rm reh}$, such as the reheating temperature and the equation of state. In fact, one can show that only one parameter is sufficient, the so-called rescaled reheating parameter R [115–119]. In the present paper, following Ref. [25], a Jeffreys prior is assumed such that $\theta_{\rm reh} = \ln R \in [-46, 15]$. Finally, the parameters describing the postinflationary phase are the standard cosmological parameters associated with a ΛCDM model, plus the astrophysical parameters entering the likelihood function. Those are referred to as $\theta_{\rm s}$ in the following. As a consequence, the evidence in Eq. (2), for a model $\mathcal{M}_i$, becomes

$$\mathcal{E}(D|\mathcal{M}_i) = \int \mathrm{d}\theta_{\rm s}\mathrm{d}\theta_{\rm reh}\mathrm{d}\theta_{\rm inf}\mathcal{L}(\theta_{\rm s}, \theta_{\rm reh}, \theta_{\rm inf}) \times \pi(\theta_{\rm s})\pi(\theta_{\rm reh})\pi(\theta_{\rm inf}), \tag{9}$$

where π represent the priors. The key remark here is to notice that, as opposed to the cosmological and astrophysics parameters, $\theta_{\rm reh}$ and $\theta_{\rm inf}$ affect the likelihood by modifying *only* the scalar $\mathcal{P}_\zeta(k)$ and tensor $\mathcal{P}_h(k)$ primordial power spectra. As a consequence, one possibility would be to numerically evaluate, for each inflationary model, $\mathcal{P}_\zeta$ and $\mathcal{P}_h$ [38,119,120]. This is, however, very time consuming.

Here, we rather choose to use the method developed in Ref. [121]. The main idea of this article is to bypass any mode integration by modeling through a small number of parameters the shape of the primordial spectra. Since we are only focused on slow-roll inflation, we consider the second order slow-roll expansion of the scalar and tensor primordial spectra around a pivot scale k_* [122–133], namely

$$\mathcal{P}_\zeta = \frac{H^2}{8\pi^2 M_{\rm Pl}^2\epsilon_1}\left\{1 - 2(1+C)\epsilon_1 - C\epsilon_2 + \left(\frac{\pi^2}{2} - 3 + 2C + 2C^2\right)\epsilon_1^2 + \left(\frac{\pi^2}{24} - \frac{C^2}{2}\right)\epsilon_2\epsilon_3 + \left(\frac{7\pi^2}{12} - 6 - C + C^2\right)\epsilon_1\epsilon_2 + \left(\frac{\pi^2}{8} - 1 + \frac{C^2}{2}\right)\epsilon_2^2 + [-2\epsilon_1 - \epsilon_2 + (2+4C)\epsilon_1^2 + (-1+2C)\epsilon_1\epsilon_2 + C\epsilon_2^2 - C\epsilon_2\epsilon_3]\ln\left(\frac{k}{k_*}\right) + \left(2\epsilon_1^2 + \epsilon_1\epsilon_2 + \frac{1}{2}\epsilon_2^2 - \frac{1}{2}\epsilon_2\epsilon_3\right)\ln^2\left(\frac{k}{k_*}\right)\right\} \tag{10}$$

and

$$\mathcal{P}_h = \frac{2H^2}{\pi^2 M_{\rm Pl}^2}\left\{1 - 2(1+C)\epsilon_1 + \left(\frac{\pi^2}{2} - 3 + 2C + 2C^2\right)\epsilon_1^2 + \left(\frac{\pi^2}{12} - 2 - 2C - C^2\right)\epsilon_1\epsilon_2 + [-2\epsilon_1 + (2+4C)\epsilon_1^2 - 2(1+C)\epsilon_1\epsilon_2]\ln\left(\frac{k}{k_*}\right) + (2\epsilon_1^2 - \epsilon_1\epsilon_2)\ln^2\left(\frac{k}{k_*}\right)\right\}, \tag{11}$$

where $C = \gamma + \ln 2 - 2 \simeq -0.72$, γ being the Euler constant. The quantities ϵ_n are the Hubble-flow parameters evaluated at the pivot Hubble exit, i.e. at the conformal time η_* solution of $k_*\eta_* = -1$. The Hubble parameter H entering the normalization is also evaluated at η_*. Let us notice that, by definition, $P_* \equiv \mathcal{P}_\zeta(k_*)$ is a well-measured quantity which fixes the amplitude of the CMB anisotropies. Let us also remark that, *a priori*, P_* is not directly proportional to $C_\ell^{\rm TT,obs}$ since, when the tensor-to-scalar ratio does not vanish, part of the signal also comes from $\mathcal{P}_h(k_*)$. However, for our choice of pivot scale, $k_* = 0.05$ Mpc^{-1}, the gravity waves contribution is already very small.

The inflationary model dependence now only appears through the explicit functionals $\epsilon_n(\theta_{\rm reh}, \theta_{\rm inf})$. These are explicitly derived for all models of the *Encyclopædia Inflationaris* in Ref. [91] and can be computed using the public library ASPIC.[4] In other words, the power spectra obtained in this way differ for different models because the functionals $\epsilon_n(\theta_{\rm reh}, \theta_{\rm inf})$ depend on the inflationary model considered. Then, the Bayesian evidence can be obtained from Eq. (9) by marginalizing over all parameters, i.e.

$$\mathcal{E}(D|\mathcal{M}_i) = \int \mathcal{L}_{\rm eff}[P_*(\theta_{\rm reh}, \theta_{\rm inf}), \epsilon_n(\theta_{\rm reh}, \theta_{\rm inf})] \times \pi(\theta_{\rm reh})\pi(\theta_{\rm inf}){\rm d}\theta_{\rm reh}{\rm d}\theta_{\rm inf}, \tag{12}$$

where we have defined the effective likelihood by

$$\mathcal{L}_{\rm eff}(P_*, \epsilon_n) \equiv \int \mathcal{L}(\theta_{\rm s}, P_*, \epsilon_n)\pi(\theta_{\rm s}){\rm d}\theta_{\rm s}. \tag{13}$$

The effective likelihood for inflation $\mathcal{L}_{\rm eff}$ is the full likelihood $\mathcal{L}$ marginalized over all the cosmological and astrophysics parameters. Its estimation therefore requires a complete data analysis that we present in the following section. However, this has to be done once and for all as the evidences of all the inflationary models can be computed afterwards from Eq. (12). In practice, the functional shape of $\mathcal{L}_{\rm eff}(P_*, \epsilon_n)$ is fitted using a neural network interpolator allowing its very fast evaluation.

[4] http://theory.physics.unige.ch/ringeval/aspic.html.

III. DATA ANALYSIS

In order to determine $\mathcal{L}_{\rm eff}$, we have performed a Markov chain–Monte Carlo (MCMC) exploration of the slow-roll parameter space using the BICEP2 and Planck likelihoods described above.

A. Constraints from BICEP2

In this first section, we derive constraints on the cosmological parameters using the BICEP2 data alone. The postinflationary universe, assumed to be a flat ΛCDM model, is described by the parameters $\theta_{\rm s}$:

$$\theta_{\rm s} = (\Omega_{\rm b}h^2, \Omega_{\rm c}h^2, \tau, 100\theta_{\rm MC}). \tag{14}$$

The cosmological parameters are the baryons energy density (normalized to the critical energy density) $\Omega_{\rm b}$, the cold dark matter energy density $\Omega_{\rm c}$, the reduced Hubble parameter today h, the optical depth τ to last scattering, and an angle, $\theta_{\rm MC}$, related to the angular size of the sound horizon on the last scattering surface [113]. The MCMC analysis was done by means of the public code COSMOMC [113] and a modified version of the CAMB code [114] taking into account that the initial power spectra are not simple power laws but are given by the expressions (10) and (11). The priors on the standard parameters are chosen in accordance with Ref. [105]. For the primordial parameters, we take a Jeffreys prior for $\ln(10^{10}P_*) \in [2.7, 4.0]$ and for ϵ_1, namely $\log(\epsilon_1) \in [-5, -0.7]$. For the other slow-roll parameters, we choose flat priors on ϵ_2 and ϵ_3 in $[-0.2, 0.2]$. As already mentioned, the pivot scale is chosen at $k_* = 0.05$ Mpc^{-1}. These priors are the most uninformative within slow-roll inflation. Indeed, the order of magnitude of ϵ_1 (which is always positive) is *a priori* unknown as many models produce a level of tensor modes that can be extremely small. This prior was the one assumed in Ref. [25].

In Fig. 3, we have represented the one-dimensional marginalized posterior probability distributions for the standard and slow-roll parameters obtained with BICEP2 data alone (solid black lines) compared with the distributions inferred from Planck (dashed red lines). It does not come as a surprise to see that, as long as the $\theta_{\rm s}$'s are concerned, BICEP2 is much less constraining than Planck. Concerning the primordial parameters, we see that BICEP2 measures ϵ_1 (or r) since it is sensitive to both the amplitude of the tensor power spectrum through $C_\ell^{\rm BB,obs}$ and the amplitude of the scalar power spectrum through $C_\ell^{\rm EE,obs}$. The quantity P_*, that is to say $\mathcal{P}(k_*)$, is indeed constrained as can be seen on the figure. On the other hand, the second and third slow-roll parameters ϵ_2 and ϵ_3 are not constrained at all.

Figure 4 shows the two-dimensional posterior probability distributions in the primordial parameter space from BICEP2 alone (solid black contours) and from Planck

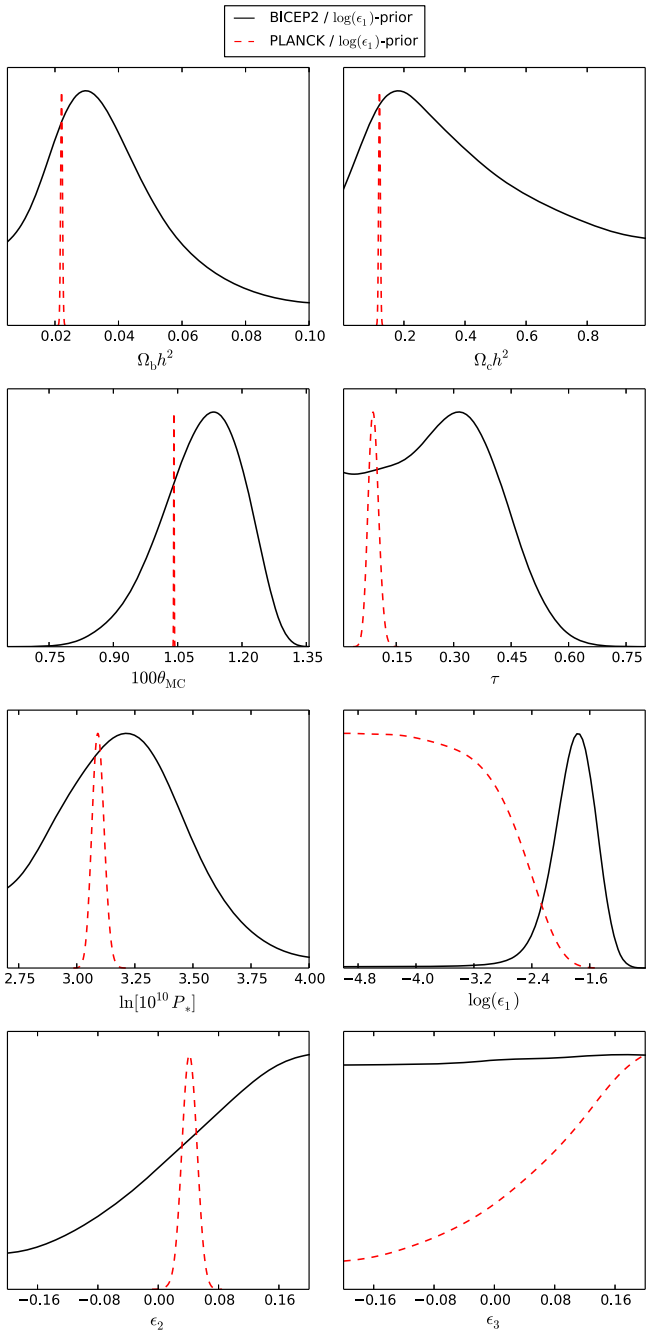

FIG. 3 (color online). One-dimensional marginalized posterior probability distributions for the cosmological and primordial slow-roll parameters obtained with BICEP2 data alone (solid black lines) compared to the corresponding Planck's posteriors (dashed red lines).

alone (red dashed contours). The upper and lower left panels are especially interesting since they illustrate the existing tension between the BICEP2 and Planck data in the sense that the one-sigma contours do not overlap (while the two-sigma contours do). Unsurprisingly, the first slow-roll parameter is well determined by BICEP2 while the second is well constrained by Planck.

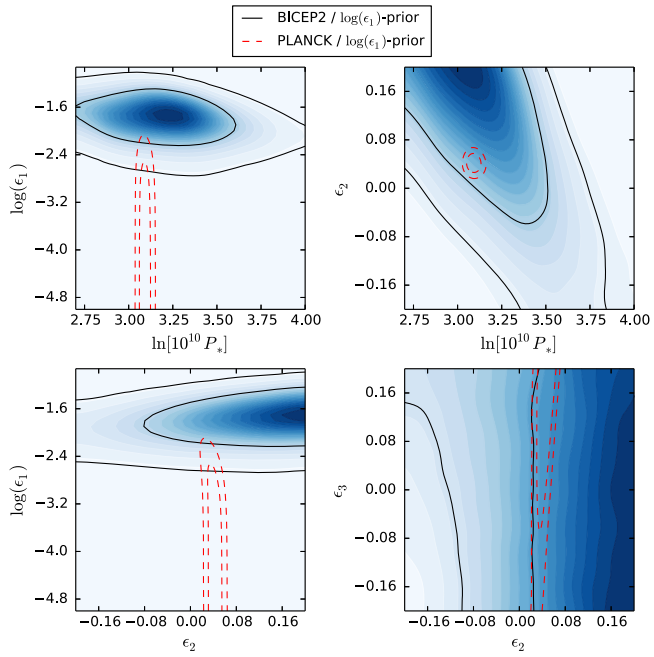

FIG. 4 (color online). Two-dimensional marginalized posterior probability distributions for the primordial slow-roll parameters obtained from BICEP2 data alone (solid black lines) compared to the corresponding Planck's posteriors (dashed red lines). The blue shading density traces the mean likelihood values for BICEP2 (Jeffreys prior on ϵ_1).

B. Constraints from BICEP2 and Planck

We now turn to the joint analysis where the BICEP2 and Planck data are simultaneously considered. The postinflationary universe is, as before, a flat ΛCDM model and is now described by a larger set of parameters θ_s:

$$\begin{aligned}\theta_s = (&\Omega_b h^2, \Omega_c h^2, \tau, 100\theta_{MC}, A_{100}^{PS}, A_{143}^{PS}, A_{217}^{PS}, r_{143\times217}^{PS},\\ &\times A_{143}^{CIB}, A_{217}^{CIB}, r_{143\times217}^{CIB}, \gamma^{CIB}, A_{tSZ},\\ &\times A_{kSZ}, \xi^{tSZ\times CIB}, c_{100}, c_{217}, \beta_1^1).\end{aligned} \quad (15)$$

The cosmological parameters are the ones already considered in the previous section, Ω_b, Ω_c, h, τ, and θ_{MC}, and their priors are the same. The remaining parameters are related to astrophysics, foregrounds, and the instrumental systematics associated with the Planck satellite. A complete description of their meaning, and priors, can be found in Ref. [105].

In order to test the robustness against prior choices, we have also performed the same slow-roll analysis but starting from a flat prior on $\epsilon_1 \in [0.00001, 0.2]$. Such a prior implicitly favors models producing a larger tensor to scalar ratio.

In Fig. 5, we have represented the marginalized posteriors for all the cosmological, astrophysics, and nuisance parameters obtained from either the Planck likelihood alone or the Planck and BICEP2 likelihoods combined. This figure also shows these posteriors in the case of our

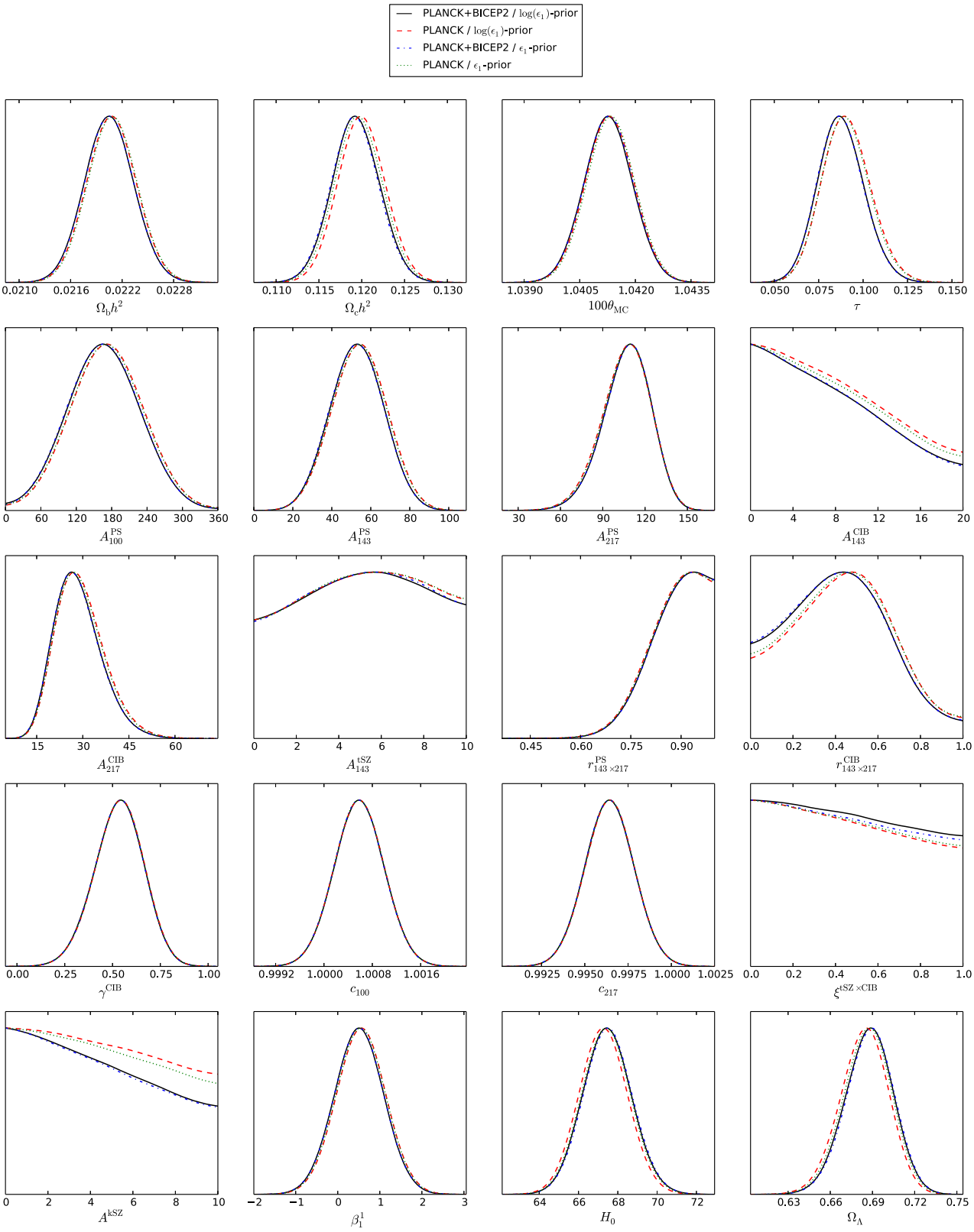

FIG. 5 (color online). One-dimensional marginalized posterior probability distributions on cosmological and astrophysics parameters associated with primordial power spectra having a second order slow-roll functional shape. These posteriors are robust against the four cases represented: Planck data alone, Planck and BICEP2 data combined, Jeffreys prior on ϵ_1, or flat prior on ϵ_1.

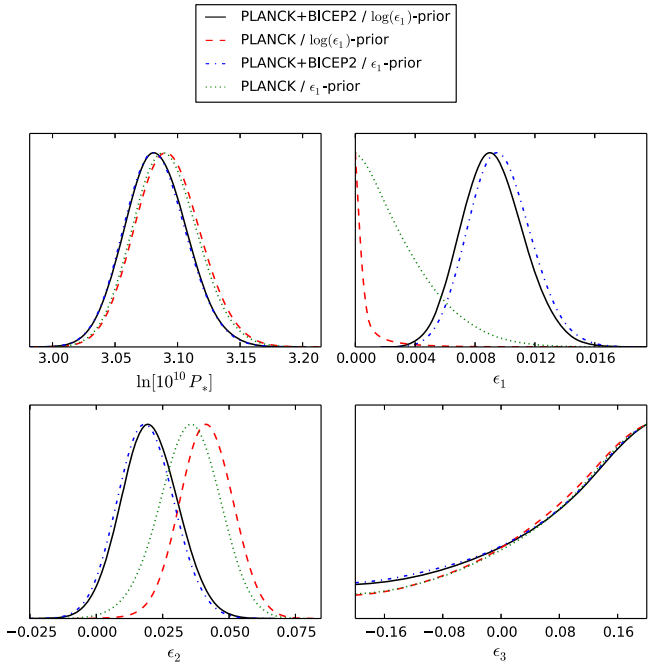

FIG. 6 (color online). One-dimensional marginalized posterior probability distributions for the primordial slow-roll parameters obtained with Planck and Planck plus BICEP2 data; with a Jeffreys prior on ϵ_1 or a flat prior on ϵ_1. Notice the one-sigma shift of the ϵ_2 posterior toward smaller values when the BICEP2 data are included.

two prior choices on ϵ_1. All of the θ_s posteriors are robust with respect to the prior choices and the combination of data used.

In Figs. 6 and 7, the one- and two-dimensional posteriors in the slow-roll parameter space have been represented for the same four combinations of prior choices and data sets. The tension between Planck and BICEP2 is particularly visible on the posterior for $\log(\epsilon_1)$ (Jeffreys prior on ϵ_1). As visible on the lower panels of Fig. 6, choosing a flat prior for ϵ_1 slightly reduces the tension but, as explained above, would implicitly favor models having a large tensor-to-scalar ratio. As expected, Planck and BICEP2 data together completely determine the first two Hubble flow functions, and one obtains the two-sigma confidence intervals

$$0.0054 < \epsilon_1 < 0.013, \qquad 0.00013 < \epsilon_2 < 0.041, \quad (16)$$

for a Jeffreys prior on ϵ_1 and

$$0.0056 < \epsilon_1 < 0.014, \qquad -0.0011 < \epsilon_2 < 0.039, \quad (17)$$

for a flat prior on ϵ_1. Because the spectral index is well constrained by Planck alone (see the discussion in Sec. III E), Figs. 6 and 7 show that combining Planck and BICEP2 also induces a one-sigma shift of the posterior for the second Hubble flow function toward vanishing

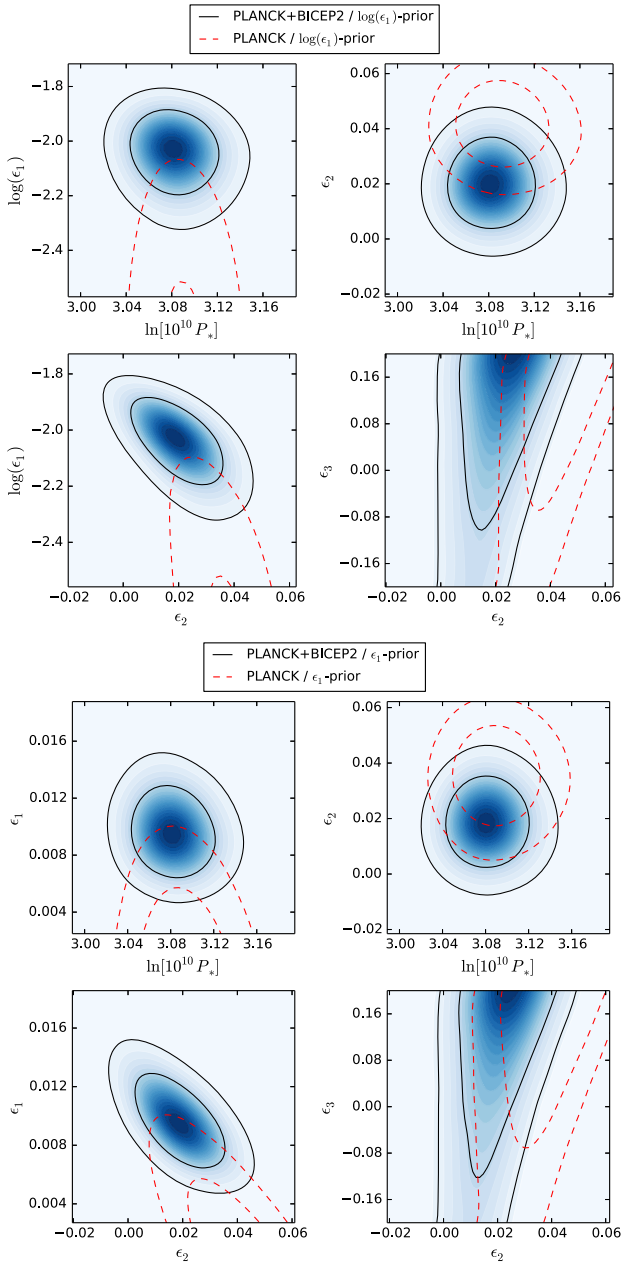

FIG. 7 (color online). One- and two-sigma contours of the marginalized posterior probability distributions for the primordial slow-roll parameters obtained with Planck and Planck+BICEP2 data. The blue shading density traces the mean likelihood values for Planck+BICEP2 (Jeffreys prior on ϵ_1). The tension between Planck and Planck + BICEP2 data induces a 1.5-sigma shift of the $\log(\epsilon_1)$ posterior toward higher values while shifting by one sigma the posterior of ϵ_2 toward zero.

values. On the contrary, the third Hubble flow function ϵ_3 remains unconstrained and unaffected by the inclusion of BICEP2.

In order to assess how much of these results come from the tension between the Planck and BICEP2 data sets, we now estimate the Bayes factor $\mathcal{R}_{SR}$ defined as the ratio

between the probability of compatibility and the probability of incompatibility.

C. Compatibility for the slow-roll model

As discussed in Sec. II B, the compatibility between BICEP2 and Planck can be evaluated from the Bayesian measure

$$\mathcal{R}_{\rm SR} = \frac{\mathcal{E}(D_{\rm p}, D_{\rm b}|{\rm SR})}{\mathcal{E}(D_{\rm p}|{\rm SR})\mathcal{E}(D_{\rm b}|{\rm SR})}, \tag{18}$$

where SR refers to the model under scrutiny, namely slow-roll. Here, we have not focused yet on a particular inflationary potential as we have sampled the whole slow-roll parameter space (in addition to the cosmological parameters). Nonetheless, this can still be interpreted as having chosen phenomenological inflationary priors that we refer to as the slow-roll model, SR. These priors have been mentioned earlier and are $\ln(10^{10}P_*) \in [2.4, 4.0]$, $\log(\epsilon_1) \in [-5, -0.7]$, $\epsilon_2 \in [-0.2, 0.2]$, and $\epsilon_3 \in [-0.2, 0.2]$, plus the standard priors for the cosmological and astrophysical parameters (see Sec. III A). Evaluating Eq. (18) requires the computation of the three integrals given by Eq. (2) for $D_{\rm p}$ (Planck), $D_{\rm b}$ (BICEP2), and $\{D_{\rm p}, D_{\rm b}\}$ (combined) which are eight-dimensional for BICEP2 and 22-dimensional for the others. This is technically nontrivial as evaluating the likelihood at each point of the parameter space requires a complete integration of the cosmological perturbations with CAMB. In order to minimize the number of likelihood evaluations and maximize convergence speed, we have used the nested sampling algorithm as implemented in MULTINEST to estimate each evidence [100,134,135]. A target accuracy of 1% has been used together with a number of live points ranging from 1000 to 20000, depending on the dimensionality of space. Moreover, for each evidence, we have performed a few runs having half the number of live points in order to estimate any systematic uncertainties. The resulting numerical estimate is

$$\ln(\mathcal{R}_{\rm SR}) = -0.01 \pm 0.4, \tag{19}$$

where the quoted error is a systematic evaluated over the various runs. In Appendix A 2, we discuss a semianalytic method to calculate $\mathcal{R}_{\rm SR}$ that requires only one integration over the BICEP2 likelihood. The result quoted in Eq. (A11) matches the above numerical value.

Such a value for $\mathcal{R}_{\rm SR}$ is very close to unity and signals equal probability of Planck and BICEP2 data to be compatible or incompatible. Let us emphasize that, on the Jeffreys' scale, strong compatibility would have required $\ln(\mathcal{R}_{\rm SR}) > 5$ while strong incompatibility would have been $\ln(\mathcal{R}_{\rm SR}) < -5$. With values of $|\ln(\mathcal{R}_{\rm SR})| < 1$, we are in the inconclusive region; namely no conclusion can be drawn on the compatibility of the two data sets. As we illustrate in Appendix A 1, the fact that we find $|\ln(\mathcal{R}_{\rm SR})| < 1$ is a nontrivial result. The tension between the Planck and BICEP2 posteriors on ϵ_1 (or r) visible in Fig. 3 ends up being compensated by the agreement between the informative posteriors for P_* and $\theta_{\rm MC}$ (see Fig. 3). Let us stress that discussing the compatibility of two data sets by estimating how much the likelihoods overlap in one direction only, without specifying any prior and without marginalizing over the other parameters, is misleading [136]. As can be seen in Fig. 9, even after marginalization, the amount of overlapping between the r posteriors is by nature prior dependent. For this reason, in the following, we will discuss the compatibility between Planck and BICEP2 by using the well defined Bayesian measure $\mathcal{R}$. In particular, even though all the *Encyclopædia Inflationaris* models belong to the slow-roll class, their prior spaces are completely different and their respective $\mathcal{R}$ values will accordingly be modified (see Fig. 15).

Since there is no evidence for incompatibility for the slow-roll model, we now derive various results applicable to the slow-roll class in general and obtained by combining Planck and BICEP2.

D. Energy scale of inflation

The correct Bayesian way to determine the energy scale of inflation is to compute the posterior distribution of the Hubble scale at the pivot crossing time, namely for the quantity H appearing in Eqs. (10) and (11). This can be done by importance sampling from the posteriors already obtained on P_*, ϵ_1, ϵ_2, and ϵ_3 [113]. From Eq. (10), one has at second order in slow roll

$$\frac{H^2}{M_{\rm Pl}^2} = 8\pi^2\epsilon_1 P_*[1 + 2(1 + C)\epsilon_1 + C\epsilon_2], \tag{20}$$

and we have plotted its posterior in Fig. 8. Assuming a Jeffreys prior on ϵ_1, Planck and BICEP2 data combined give the two-sigma confidence interval

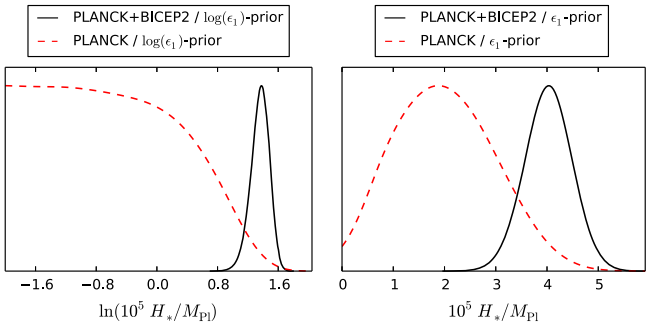

FIG. 8 (color online). Marginalized posterior distribution for the inflationary Hubble parameter at the time of pivot crossing. BICEP2 measures the energy scale of inflation.

$$1.1 < \ln\left(10^5 \frac{H}{M_{\rm Pl}}\right) < 1.6, \tag{21}$$

with a mean value at $\ln(10^5 H/M_{\rm Pl}) = 1.36$, namely $H \simeq 9.5 \times 10^{13}$ GeV. Starting from a flat prior on ϵ_1, one obtains instead

$$3.1 < 10^5 \frac{H}{M_{\rm Pl}} < 4.9, \tag{22}$$

and a mean value at $10^5 H/M_{\rm Pl} = 4.02$, giving $H \simeq 9.8 \times 10^{13}$ GeV. Those values can be converted into gravitating energy scales through the Friedmann-Lemaître equation, i.e.

$$\rho_*^{1/4} = 3^{1/4}\sqrt{H M_{\rm Pl}}. \tag{23}$$

One finds the corresponding values $\rho_*^{1/4} \simeq 2.00 \times 10^{16}$ GeV (Jeffreys prior on ϵ_1) and $\rho_*^{1/4} \simeq 2.03 \times 10^{16}$ GeV (flat prior on ϵ_1).

E. Power law derived parameters

Similarly, as it is explicit from Eqs. (10) and (11), the spectral indices $n_{\rm S}$ and $n_{\rm T}$, the tensor-to-scalar ratio r and the runnings $\alpha_{\rm S}$ and $\alpha_{\rm T}$ are completely given in terms of the Hubble flow functions. At second order in slow roll, the spectral indices read [132,133]

$$\begin{aligned} n_{\rm S} &= 1 - (2\epsilon_1 + \epsilon_2) - 2\epsilon_1^2 - (3 + 2C)\epsilon_1\epsilon_2 - C\epsilon_2\epsilon_3, \\ n_{\rm T} &= -2\epsilon_1 - 2\epsilon_1^2 - 2(1 + C)\epsilon_1\epsilon_2, \end{aligned} \tag{24}$$

while the tensor-to-scalar ratio can be expressed as

$$r = 16\epsilon_1(1 + C\epsilon_2). \tag{25}$$

The scalar and tensor running are given by

$$\alpha_{\rm S} = -2\epsilon_1\epsilon_2 - \epsilon_2\epsilon_3, \qquad \alpha_{\rm T} = -2\epsilon_1\epsilon_2, \tag{26}$$

respectively. Finally, let us mention that the running of the running for the tensor mode is also completely specified by the first three Hubble flow functions and reads

$$\beta_{\rm T} = -2\epsilon_1\epsilon_2(\epsilon_2 + \epsilon_3). \tag{27}$$

At leading order in slow roll, those equations can be recast into the so-called consistency relations

$$\begin{aligned} r &\simeq -8 n_{\rm T}, \\ \alpha_{\rm T} &\simeq \frac{r}{8}\left[\frac{r}{8} + (n_{\rm S} - 1)\right], \\ \beta_{\rm T} &\simeq \alpha_{\rm T}(1 - n_{\rm S}) + \frac{r}{8}(\alpha_{\rm S} - 2\alpha_{\rm T}). \end{aligned} \tag{28}$$

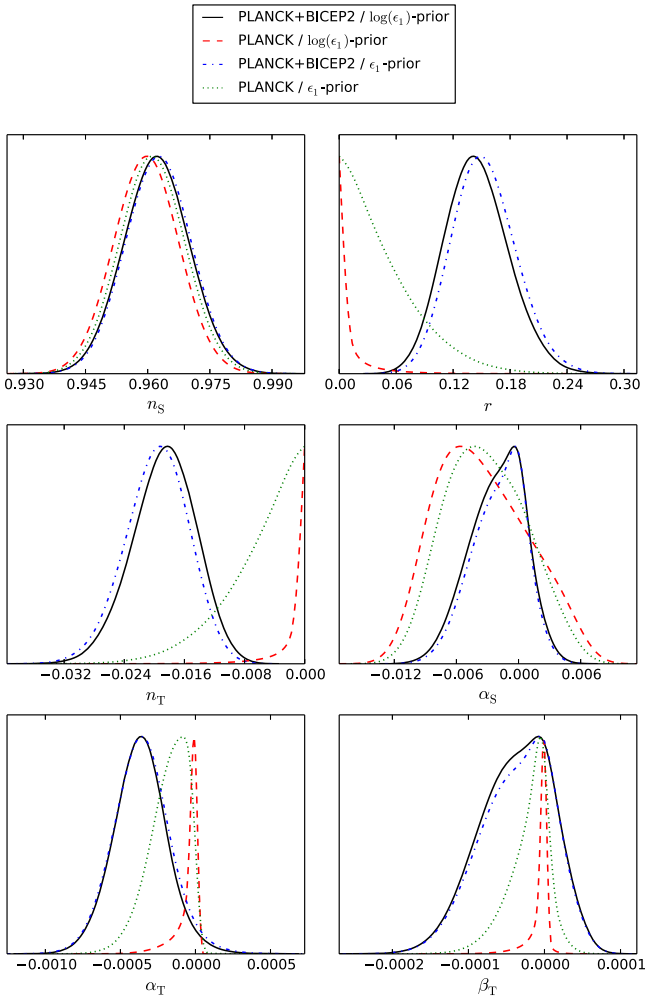

FIG. 9 (color online). Marginalized posterior distribution for the derived power law parameters $n_{\rm S}$, r, $n_{\rm T}$, $\alpha_{\rm S}$, $\alpha_{\rm T}$, and $\beta_{\rm T}$ obtained by importance sampling from the second order slow-roll parameters. Within slow-roll inflation, the running $\alpha_{\rm S}$ is more tightly constrained when the BICEP2 data are included.

Using again importance sampling, the posterior distributions for $n_{\rm S}$, $n_{\rm T}$, r, $\alpha_{\rm S}$, $\alpha_{\rm T}$, and $\beta_{\rm T}$ have been represented in Figs. 9 and 10. In particular, let us stress that, within slow-roll inflation, a running spectral index for the scalar modes cannot help to alleviate the tension between Planck and BICEP2 data. On the contrary, we see that the posterior of $\alpha_{\rm S}$ is more restricted around vanishing values by adding the BICEP2 data. As it is explicit in Eq. (26), $\alpha_{\rm S}$ is a small quantity which is proportional to ϵ_2, the posterior of which is being shifted toward 0 when the BICEP2 data are considered (see Sec. III B). From this equation one has

$$|\alpha_{\rm S}|_{\rm max} \simeq |\epsilon_2|_{\rm max}(2|\epsilon_1|_{\rm max} + |\epsilon_3|_{\rm max}) \simeq |\epsilon_2|_{\rm max}|\epsilon_3|_{\rm max}, \tag{29}$$

the third Hubble flow function ϵ_3 being the largest term since it is unconstrained [$\max(|\epsilon_3|) = 0.2$]. Therefore,

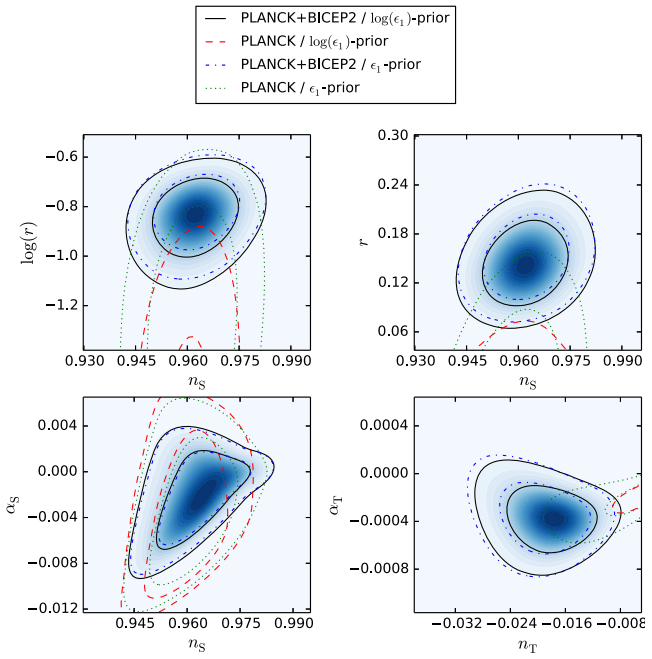

FIG. 10 (color online). Two-dimensional posterior distribution for some of the derived power law parameters. The blue shading density traces the mean likelihood values for Planck + BICEP2 (Jeffreys prior on ϵ_1).

shifting ϵ_2 toward small values implies the same for α_S. This effect could have been expected as Planck alone strongly constrains the spectral index, which is given by Eq. (24). Increasing ϵ_1 at fixed n_S imposes to decrease ϵ_2 by twice the amount. Therefore, Eq. (29) implies that the maximal values of $|\alpha_S|$ will be accordingly reduced.

From the posteriors represented in Fig. 9, Planck and BICEP2 data combined yield the following 95% confidence intervals

$$0.947 < n_S < 0.978, \qquad -0.0074 < \alpha_S < 0.0025,$$
$$-1.07 < \log(r) < -0.67, \qquad -0.027 < n_T < -0.011, \tag{30}$$

and

$$-7.1 \times 10^{-4} < \alpha_T < -3.1 \times 10^{-6},$$
$$-1.3 \times 10^{-4} < \beta_T < 5.0 \times 10^{-5}, \tag{31}$$

when a Jeffreys prior is assumed on ϵ_1. These bounds are relatively robust against the prior choices. Indeed, assuming instead a flat prior on ϵ_1 gives

$$0.947 < n_S < 0.978, \qquad -0.0071 < \alpha_S < 0.0027,$$
$$0.088 < r < 0.22, \qquad -0.028 < n_T < -0.011, \tag{32}$$

and

$$-7.1 \times 10^{-4} < \alpha_T < 2.7 \times 10^{-5},$$
$$-1.3 \times 10^{-4} < \beta_T < 5.0 \times 10^{-5}. \tag{33}$$

To conclude this section, let us stress that although there is a tension between the Planck and BICEP2 data on the tensor-to-scalar ratio, it does not affect the posterior values of the cosmological and astrophysics parameters, those being already strongly constrained by the Planck data alone. Concerning the shape of the primordial power spectra, n_S remains also unaffected while the tensor-to-scalar ratio tension induces a drastic modification of the ϵ_1 posterior distribution and a one- to two-sigma shift of the ϵ_2 distribution compared to the Planck data alone. Moreover, as we have just discussed, the running of the scalar power spectrum cannot be used within slow-roll inflation to alleviate the above-mentioned tension, precisely because it cannot take large enough values. Solely in slow-roll violating models of inflation, such an explanation may be relevant [137–141].

Concerning the implications for inflation, BICEP2 results provide, for the first time, a measure of the energy scale of inflation which ends up being at GUT scale [see Eqs. (22) and (23)], a major result indeed if confirmed. The mean value of $r = 0.15$ is slightly lower than what was inferred by the BICEP2 team, but this is expected as we are here considering slow-roll inflation and have added the Planck data which disfavor larger tensor-to-scalar ratio values. As for the evidences, one should therefore expect all models predicting a very small tensor-to-scalar ratio to be now strongly penalized evidence-wise. That is why, if the BICEP2 measurements stand the test of time, this situation would be a pivotal moment for cosmic inflation models.

In the following, we use the multidimensional posterior on P_* and ϵ_i, derived under the Jeffreys prior on ϵ_1, coming from the BICEP2 data as our effective likelihood $\mathcal{L}_{\rm eff}$.

IV. RESULTS AND DISCUSSION

In this section, we apply the method described previously in order to derive the Bayesian evidences and complexities for the $N^{\rm mod} = 193$ models of the *Encyclopædia Inflationaris*. The complete list of models as well as a careful discussion and justification of the priors on the free parameters $\theta_{\rm inf}$ can be found in Ref. [25]. In the present article, we use the same terminology and the same choices for the priors.

A. BICEP2 evidences

In Fig. 11, we show the (logarithm) of the Bayes factors, $B^i_{\rm SR}$, normalized to the slow-roll model, and computed with the BICEP2 data only. The value of $\ln B^i_{\rm SR}$ is represented by a horizontal bar on the left if $\ln B^i_{\rm SR} < 0$ (the model $\mathcal{M}_i$ is disfavored with respect to the slow-roll model) and by a horizontal bar on the right if $\ln B^i_{\rm SR} > 0$ (the model $\mathcal{M}_i$ is favored with respect to the slow-roll model), the length of

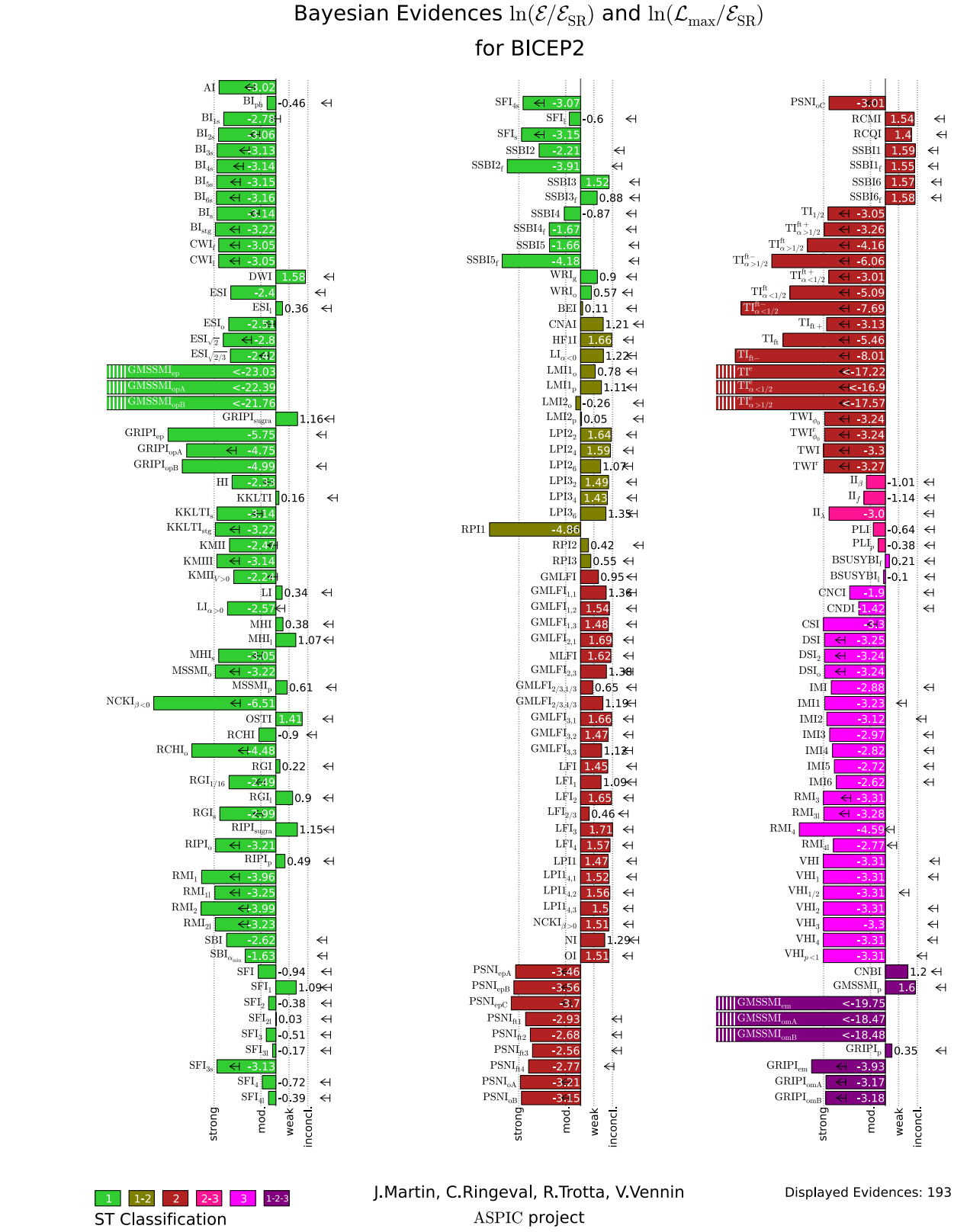

FIG. 11 (color online). Bayes factors and absolute upper bounds to the Bayes factors obtained from the BICEP2 data alone. The reference model is the slow-roll model (SR), here viewed as a scenario in itself having three parameters $\ln(10^{10}P_*)$, $\log(\epsilon_1)$, and ϵ_2 and whose priors are reported in the text. The vertical dotted lines refer to the Jeffreys scale with respect to the best model, here LFI3.

the bar being directly proportional to $\ln B^i_{\rm SR}$. There is also a color code which indicates the Schwarz Terrero–Escalante classification [142]. Let us briefly recall that, according to this classification, category one ("green" models) corresponds to models for which the kinetic energy and the kinetic to total energy ratio increases during inflation. Typically, this region contains models having a plateau shape potential. As shown in Ref. [25], this class of models is favored by the Planck data (see below). Category two ("red" models) contains models for which the kinetic energy decreases but the kinetic to total energy ratio increases during inflation. Large field models belongs to this region. Finally, category three ("purple" models) refers to models having a decreasing kinetic and kinetic to total energy ratio. Valley hybrid inflation is an example of a model belonging to this category; for a more detailed explanation of this classification and its meaning, see Ref. [25]. We have also computed the maximum value of the evidences obtained when all the parameters have a Dirac function prior peaked at the best fit. This is indicated by the small black arrows. They can be interpreted as upper bounds on the evidences regardless of the priors. Finally the vertical dotted black lines refer to the Jeffreys scale with respect to the best model and represent the four different categories, "inconclusive" (models between the first and the second vertical lines, starting from the right), "weakly disfavored" (between the second and the third vertical lines), "moderately disfavored" (between the third and the fourth vertical lines), and "strongly disfavored" (left to the fourth vertical line); see Table 1 in Ref. [25].

As can be seen in Fig. 11, the best model according to BICEP2 is LFI_3, for which $V(\phi) \propto \phi^3$. We see that there are in fact 52 models in the inconclusive zone (this one being defined with respect to the best model), namely LFI_3, $\mathrm{GLMFI}_{2,1}$, HF1I, $\mathrm{GMLFI}_{3,1}$, LFI_2, $\mathrm{LPI2}_2$, MLFI, $\mathrm{GMSSMI}_{\rm p}$, SSBI1, $\mathrm{LPI2}_4$, $\mathrm{SSBI6}_{\rm f}$, DWI, LFI_4, SSBI6, $\mathrm{LPI1}_{4,2}$, $\mathrm{SSBI1}_{\rm f}$, $\mathrm{GMLFI}_{1,2}$, RCMI, $\mathrm{LPI1}_{4,1}$, SSBI3, OI, $\mathrm{NCKI}_{\beta>0}$, $\mathrm{LPI1}_{4,3}$, $\mathrm{LPI3}_2$, $\mathrm{GMLFI}_{1,3}$, LPI1, $\mathrm{GMLFI}_{3,2}$, LFI, $\mathrm{LPI3}_4$, OSTI, RCQI, $\mathrm{GMLFI}_{2,3}$, $\mathrm{GMLFI}_{1,1}$, $\mathrm{LPI3}_6$, NI, $\mathrm{LI}_{\alpha<0}$, CNAI, CNBI, $\mathrm{GMLFI}_{2/3,4/3}$, $\mathrm{GRIPI}_{\rm sugra}$, $\mathrm{RIPI}_{\rm sugra}$, $\mathrm{GMLFI}_{3,3}$, $\mathrm{LMI1}_{\rm p}$, LFI_1, SFI_1, $\mathrm{LPI2}_6$, MHI_1, GMLFI, $\mathrm{WRI}_{\rm g}$, RGI_1, $\mathrm{SSBI3}_{\rm f}$ and $\mathrm{LMI1}_{\rm o}$, where we have ordered the list in decreasing values of the evidences.

Let us now discuss these potentials and the physical context in which they arise. CNAI, CNBI, HF1I, $\mathrm{LMI1}_{\rm o}$, and MHI_1 are phenomenological and, therefore, difficult to embed in high energy physics. LFI is just the general family of monomial potentials $V(\phi) \propto \phi^p$, and, in the inconclusive zone, one finds LFI_3, LFI_2, LFI_4, and LFI_1. The $\mathrm{GMLFI}_{p,q}$ potentials (this includes MLFI for which $p = q = 2$) are of the form $V(\phi) \propto (\phi/M_{\rm Pl})^p [1 + \alpha(\phi/M_{\rm Pl})^q]$, where α is a parameter controlling the amplitude of the second term. Physically, they could represent LFI modified by some quantum corrections [143–145]. The following potentials can also be viewed as large field corrected models: RCMI, $V(\phi) \propto (\phi/M_{\rm Pl})^2 [1 - 2\alpha(\phi/M_{\rm Pl})^2 \ln(\phi/M_{\rm Pl})]$ and RCQI, $V(\phi) \propto (\phi/M_{\rm Pl})^4 [1 - \alpha \ln(\phi/M_{\rm Pl})]$. DWI has a $V(\phi) \propto [(\phi/\phi_0) - 1]^2$ which is the sum of three monomials but was mainly used in the context of topological inflation. In the inconclusive zone, one also finds the SSBI potentials which are given by $V(\phi) \propto 1 + \alpha(\phi/M_{\rm Pl})^2 + \beta(\phi/M_{\rm Pl})^4$ and can be viewed as models where the vacuum energy part of the potential is corrected by higher order monomial terms. This is also the case for $\mathrm{NCKI}_{\beta>0}$, $V(\phi) \propto 1 + \alpha \ln(\phi/M_{\rm Pl}) + \beta(\phi/M_{\rm Pl})^2$ where the corrections are also of radiative origin and loop inflation $\mathrm{LI}_{\alpha<0}$, $V(\phi) =\propto [1 + \alpha \ln(\phi/M_{\rm Pl})]$ with $\alpha < 0$. Another class of models that are among the BICEP2 winners is LPI's, $V(\phi) \propto (\phi/\phi_0)^p [\ln(\phi/\phi_0)]^q$. These scenarios are based on super Yang-Mills theories and are also known as glueball inflation. Notice, however, that the value of ϕ_0 must be super-Planckian. The model OI, $V(\phi) \propto (\phi/\phi_0)^4 [\ln^2(\phi/\phi_0) - \alpha]$, possesses a similar potential as well as OSTI, $V(\phi) \propto (\phi/\phi_0)^2 \ln[(\phi/\phi_0)^2]$. This last scenario is physically well motivated in the context of string theory. Unfortunately, it is used outside its natural domain of validity since Ref. [146] showed that it has severe problems in matching the amplitude of the CMB anisotropies. In the inconclusive zone, one also finds inflection point models such as $\mathrm{GMSSMI}_{\rm p}$, $\mathrm{RIPI}_{\rm sugra}$, and $\mathrm{GRIPI}_{\rm sugra}$. Some of them are also used in a nonphysical region. For instance, this is the case for $\mathrm{GMSSMI}_{\rm p}$, $V(\phi) \propto (\phi/\phi_0)^2 - 2\alpha/3(\phi/\phi_0)^6 + \alpha/5(\phi/\phi_0)^5$. The model is based on the minimal supersymmetric standard model (MSSM) where the inflaton field evolves along a flat direction and is, therefore, well justified from a high energy point of view. However, in order to be a satisfactory inflationary model, ϕ_0 must have a vacuum expectation value that is outside the natural MSSM values. RGI_1 refers to radion gauge inflation and has a potential given by $V(\phi) \propto (\phi/M_{\rm Pl})^2/[\alpha + (\phi/M_{\rm Pl})^2]$. SFI_1 is nothing but small field inflation, $V(\phi) \propto 1 - (\phi/\mu)^p$, with $p = 1$. Finally, natural inflation (NI), for which $V(\phi) \propto 1 + \cos(\phi/f)$ is also a good model but must be used in a domain where the scale f is super-Planckian.

We have also computed the Bayesian complexities [see Eq. (3)] for all the *Encyclopædia Inflationaris* models, so that the performance of a model can be described by two numbers, its evidence and its complexity or equivalently see Eq. (5), its evidence and its number of unconstrained parameters. We have represented the corresponding result in the space $[N^{\rm uc}, \ln(\mathcal{E}/\mathcal{E}_{\rm best})]$ in Fig. 12. If one restricts oneself to models in the "inconclusive zone" with a minimal number of unconstrained parameters, i.e. $0 < N^{\rm uc}_i < 1$, then one finds only 17 models, namely LFI_3, LFI_2, DWI, LFI_4, RCMI, OSTI, RCQI, $\mathrm{GMLFI}_{1,1}$, NI, $\mathrm{LI}_{\alpha<0}$, CNBI, $\mathrm{GMLFI}_{2/3,4/3}$, $\mathrm{RIPI}_{\rm sugra}$, SFI1, MHI_1, $\mathrm{WRI}_{\rm g}$, and RGI_1. It is interesting to notice that the $V(\phi) = m^2\phi^2/2$ model (i.e. LFI_2) is among the models favored by

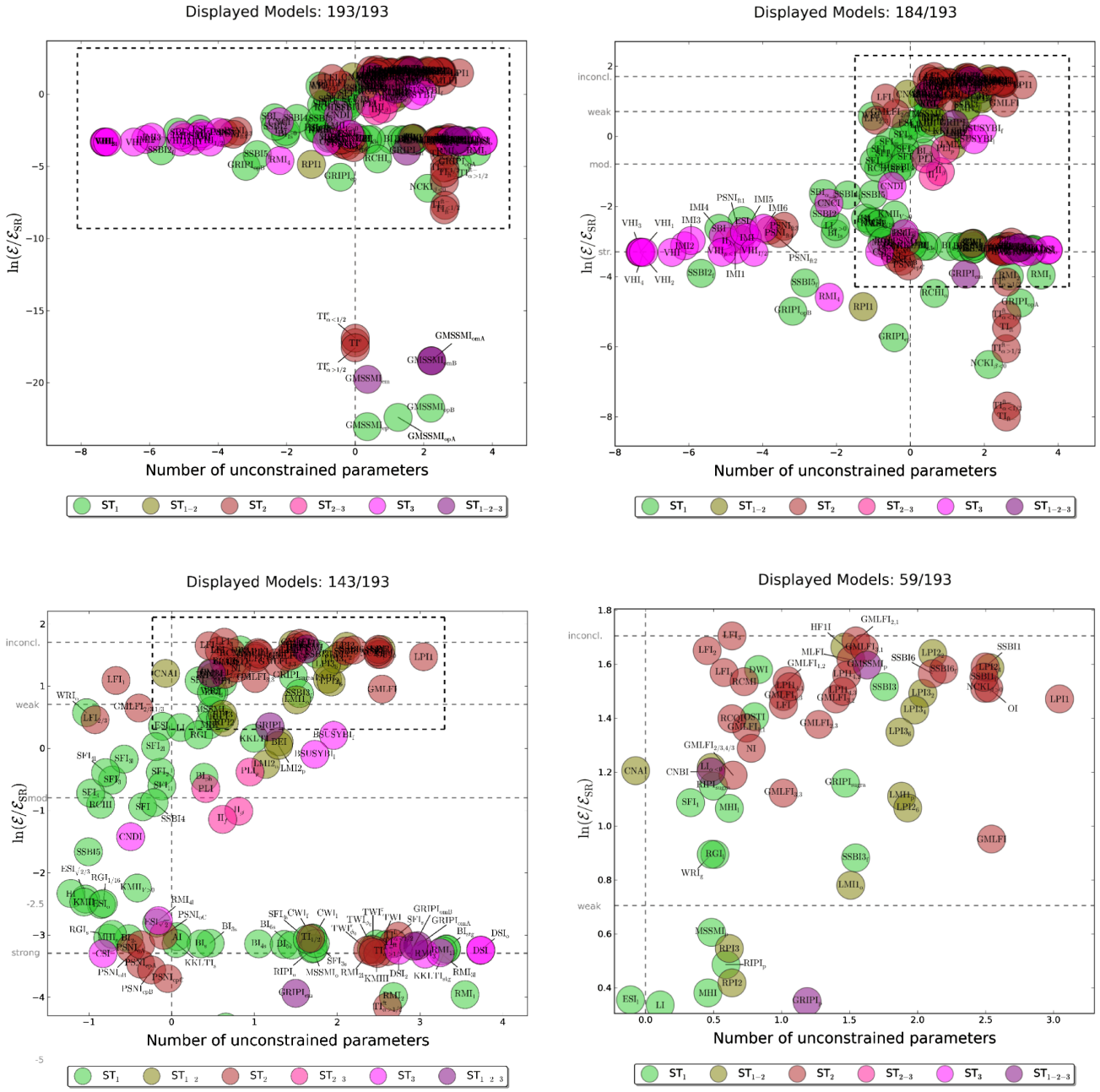

FIG. 12 (color online). Model performance assessed with both Bayesian evidence and number of unconstrained parameters for the BICEP2 data. The four panels represent different zooms in the models' space. They are to be read from the left to the right and from the top to the bottom—in this order, the black dashed rectangles frame the region comprised in the next panel.

BICEP2 but is not the only one. At this stage, it would therefore be unjustified to focus model building efforts on this scenario only.

In order to compare the above results with what has been obtained by Planck, we have reproduced in Fig. 13 the values of the evidences, normalized to the slow-roll model, obtained with the Planck data in Ref. [25]. This figure is identical to Fig. 2 of Ref. [25] except that the reference model is now different (being HI in [25]). The best Planck model is KMIII and the 52 models that end up being in the inconclusive zone (with respect to the best) are KMIII, $\mathrm{ESI}_{\sqrt{2}}$, $\mathrm{BI}_{6\mathrm{s}}$, $\mathrm{MHI}_{\mathrm{s}}$, BI_{s}, ESI, $\mathrm{BI}_{5\mathrm{s}}$, $\mathrm{KKLTI}_{\mathrm{s}}$, $\mathrm{KMII}_{V>0}$, $\mathrm{BI}_{4\mathrm{s}}$, $\mathrm{ESI}_{\mathrm{o}}$, $\mathrm{ESI}_{\sqrt{2/3}}$, KMII, HI, $\mathrm{BI}_{3\mathrm{s}}$, $\mathrm{BI}_{2\mathrm{s}}$, $\mathrm{RGI}_{\mathrm{s}}$, $\mathrm{RGI}_{1/16}$, $\mathrm{BI}_{\mathrm{ph}}$, AI, $\mathrm{BI}_{1\mathrm{s}}$, MHI, SFI_1, SFI, $\mathrm{KKLTI}_{\mathrm{stg}}$, $\mathrm{BI}_{\mathrm{stg}}$, KKLTI, SBI, RGI, $\mathrm{SFI}_{\mathrm{s}}$, $\mathrm{PSNI}_{\mathrm{oA}}$, $\mathrm{SFI}_{4\mathrm{l}}$, $\mathrm{PSNI}_{\mathrm{ft2}}$, $\mathrm{PSNI}_{\mathrm{oB}}$, $\mathrm{PSNI}_{\mathrm{ft1}}$, $\mathrm{PSNI}_{\mathrm{oC}}$, $\mathrm{LI}_{\alpha>0}$, SFI_4, ESI_1, SSBI2, $\mathrm{PSNI}_{\mathrm{ft3}}$, $\mathrm{PSNI}_{\mathrm{epA}}$, SSBI4, $\mathrm{TWI}_{\phi 0}$, RGI_1, $\mathrm{SFI}_{4\mathrm{s}}$, MHI_1, $\mathrm{PSNI}_{\mathrm{epB}}$, $\mathrm{TWI}^{\Gamma}_{\phi 0}$, $\mathrm{SBI}_{\alpha_{\mathrm{min}}}$, LI, $\mathrm{SFI}_{3\mathrm{l}}$.

Two remarks are in order here. First, the number of models favored is exactly the same for BICEP2 and Planck,

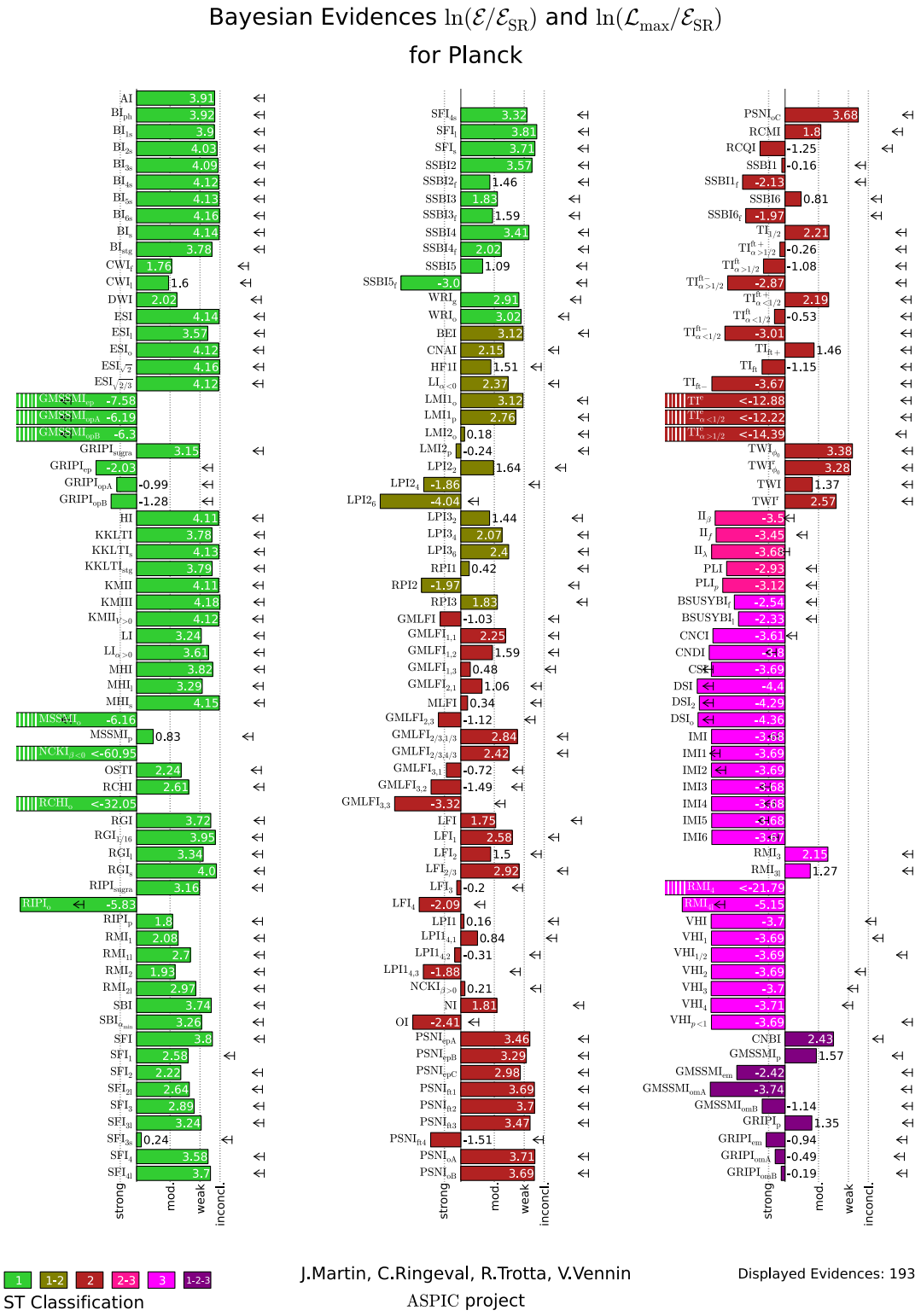

FIG. 13 (color online). Bayes factors and absolute upper bounds to the Bayes factors obtained from the Planck data as in Ref. [25]. The reference model is the same slow-roll model as in Fig. 11, and the vertical dotted lines refer to the Jeffreys scale with respect to the best model, here KMIII.

namely 52. This probably illustrates the fact that r is an observable which is able to discriminate among the inflationary models much more efficiently that n_S. Indeed, as mentioned above, we have used only four band powers for the BICEP2 data, and this already singles out the same number of scenarios in the inconclusive zone. Second, there are only two models belonging to the two lists: MHI_1 and RGI_1. In particular, the fact that the Starobinsky (or Higgs) inflationary model was among the winners according to Planck is not recovered by BICEP2. On the contrary, this one becomes (almost) strongly disfavored compared to LFI_3.

In Ref. [25], the complexity was also calculated; see Fig. 3 of that article. We found that, among the models in the Planck inconclusive zone, those with a minimal number of unconstrained parameters, i.e. $0 < N_i^{\mathrm{uc}} < 1$, are $\mathrm{ESI}_{\sqrt{2}}$, $\mathrm{ESI}_{\sqrt{2/3}}$, HI, BI_{2s}, RGI_s, AI, BI_{1s}, MHI, RGI, SFI_{4l}, $\mathrm{LI}_{\alpha>0}$, SFI_4, ESI_1, RGI_1, MHI_1, $\mathrm{SBI}_{\alpha_{\mathrm{min}}}$, and SFI_{3l}. Again, two models remain in the two lists, the same as above, namely MHI_1 and RGI_1.

Finally, we can summarize the data constraining power in a histogram for the four Jeffreys categories as represented in Fig. 14. We have also represented the same histogram obtained from the Planck data. Noticing again that the BICEP2 data used here consist only of four band powers for E and B modes, this plot illustrates the power of measuring r for inflationary physics. However, as discussed earlier, the models lying in these four categories weakly overlap between Planck and BICEP2 thereby showing some tension between the data sets. Since compatibility between data sets is a model dependent statement, we now move on to the determination of the $\mathcal{R}$ factors for all the *Encyclopædia Inflationaris* models.

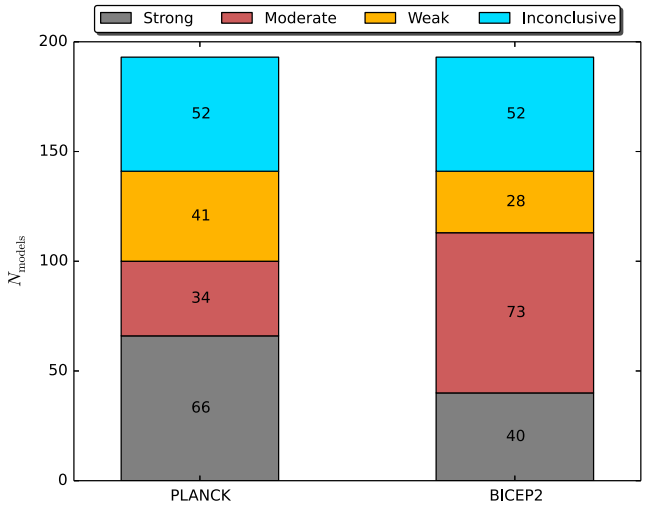

FIG. 14 (color online). Number of models within each Jeffreys category (with respect to the best model) for Planck data alone and BICEP2 data alone.

B. Compatibility of Planck and BICEP2

In Fig. 15 we have represented the values of $\ln(\mathcal{R})$ for all the *Encyclopædia Inflationaris* models. These have been obtained using the fast likelihood method described in Sec. II. In this plot, one notices that the data sets are compatible with certainty [i.e. at the "strong" level, $\ln(\mathcal{R}) > 5$] for 36 models only. They are $\mathrm{GMSSMI}_{\mathrm{opA}}$, $\mathrm{GMSSMI}_{\mathrm{opB}}$, $\mathrm{GMSSMI}_{\mathrm{ep}}$, TI^{e}, $\mathrm{TI}^{\mathrm{e}}_{\alpha>1/2}$, $\mathrm{TI}^{\mathrm{e}}_{\alpha<1/2}$, II_β, II_f, II_λ, PLI, PLI_p, $\mathrm{BSUSYBI}_{\mathrm{f}}$, $\mathrm{BSUSYBI}_{\mathrm{l}}$, CSI, DSI, DSI_2, DSI_2, $\mathrm{DSI}_{\mathrm{o}}$, IMI, IMI1, IMI2, IMI3, IMI4, IMI5, IMI6, RMI_4, $\mathrm{RMI}_{4\mathrm{l}}$, VHI, VHI_1, $\mathrm{VHI}_{1/2}$, VHI_2, VHI_3, VHI_4, $\mathrm{VHI}_{p<1}$, $\mathrm{GMSSMI}_{\mathrm{em}}$, $\mathrm{GMSSMI}_{\mathrm{omA}}$, and $\mathrm{GMSSMI}_{\mathrm{omB}}$. As one can check in Figs. 11 and 13, these models are disfavored by both Planck and BICEP2 separately; the ones exhibiting maximum compatibility are even ruled out. This is not surprising as $\mathcal{R}$ is a combined measure of both the reduction of prior volume brought about by the likelihood as well as their overlap (see Appendix A 1). The statistical interpretation of these results is that both data sets agree in disfavoring those models.

On the other hand, one may be more interested in answering the question whether the data sets are compatible assuming the best Planck's scenarios. In Fig. 16, we have represented the same $\mathcal{R}$ factors of Fig. 15 plotted against the Bayes factor derived from the Planck data alone (the ones of Fig. 13). The shaded rectangles (yellow) trace the overlapping regions of maximal evidence and maximal compatibility over two units in the Jeffreys scale: inconclusive plus weak zones along the evidence direction and strong plus moderate zones along the compatibility direction. There is no model in these regions showing that, insofar the best inflationary models from Planck data alone are concerned, the two data sets are in tension. In fact, only a weak compatibility is reached for models which are already weakly disfavored by the Planck data alone. Many of these models belong to the ones listed earlier that were favored by BICEP2 alone (as $\mathrm{NI}, \mathrm{SSBI3}, \mathrm{RIPI}_{\mathrm{p}}, \ldots$).

For the Planck best models, the BICEP2 data cannot be brought into compatibility with Planck, and hence the two data sets cannot be combined to obtain meaningful updated inferences on these scenarios. In particular, this is the conclusion for Starobinsky inflation (HI), and, therefore, it is premature to conclude about its viability before compatibility is addressed. As we have just showed, both data sets can be meaningfully combined only if one focuses on scenarios which are, at least, weakly disfavored by Planck.

It is also informative to assess the compatibility of the two data sets from the perspective of the BICEP2 best models. In Fig. 17 we have plotted the analog of Fig. 16 for BICEP2, namely the $\mathcal{R}$ factors against the Bayes factors obtained from BICEP2 data alone (see Fig. 11). The BICEP2 best scenarios now spread into the region of moderate compatibility although there is again no model in the strong compatibility region. Nonetheless,

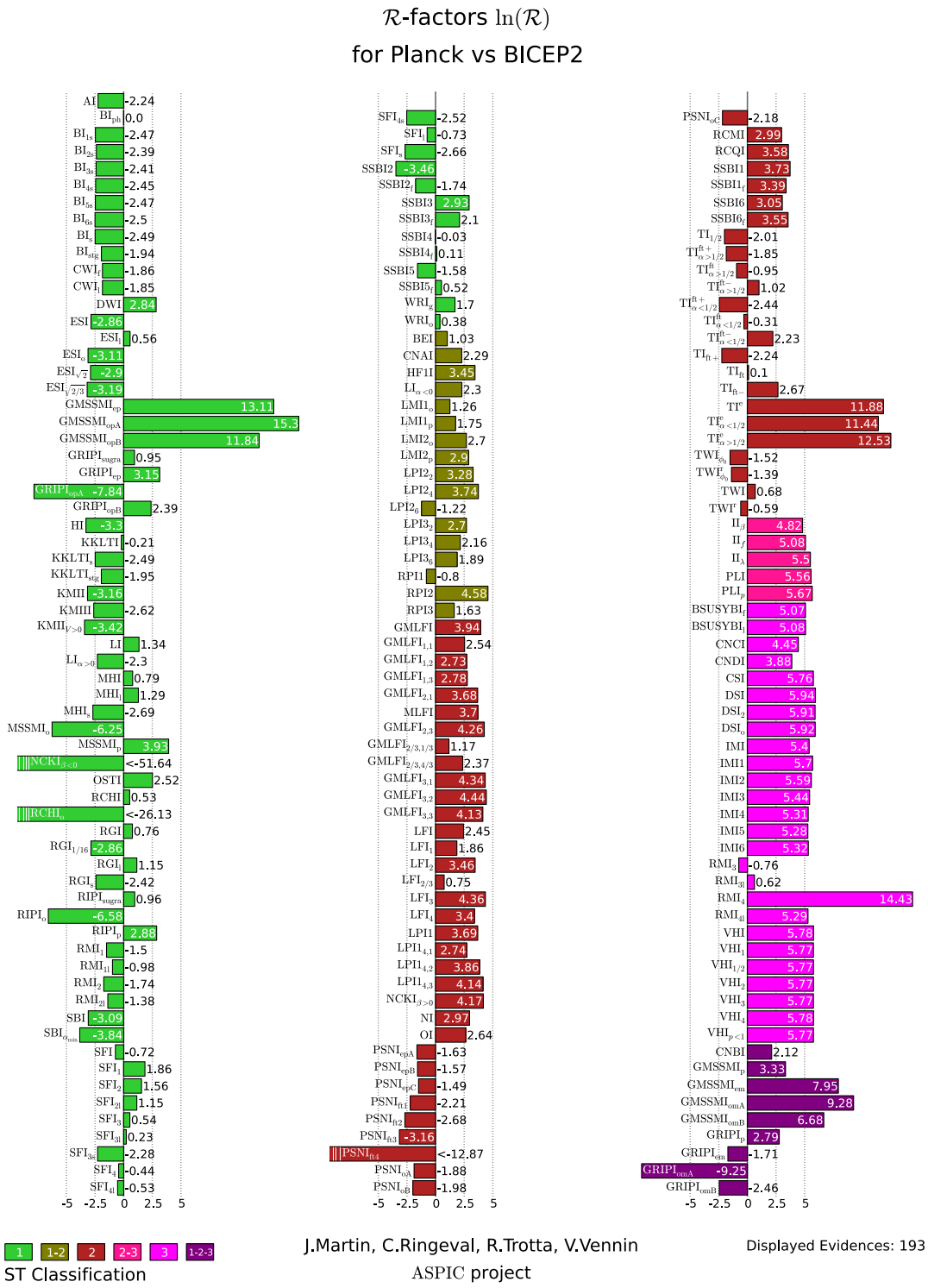

FIG. 15 (color online). Compatibility between the Planck and BICEP2 data for each model as measured by the $\mathcal{R}$ factors. Positive values correspond to compatibility, negative values to incompatibility.

for the BICEP2 best scenarios, Planck and BICEP2 data can be combined to get more information for these scenarios.

In the light of the above considerations, in Fig. 18 we have represented the Bayes factors obtained by combining Planck and BICEP2 together, but only for models having $\mathcal{R} > 1$ since combining models with $\mathcal{R} < 1$ is meaningless. Our chosen threshold of $\mathcal{R}$ is conservative (i.e. we are not requiring $\mathcal{R} \gg 1$), and it includes scenarios under which, in the present situation, one cannot conclude about

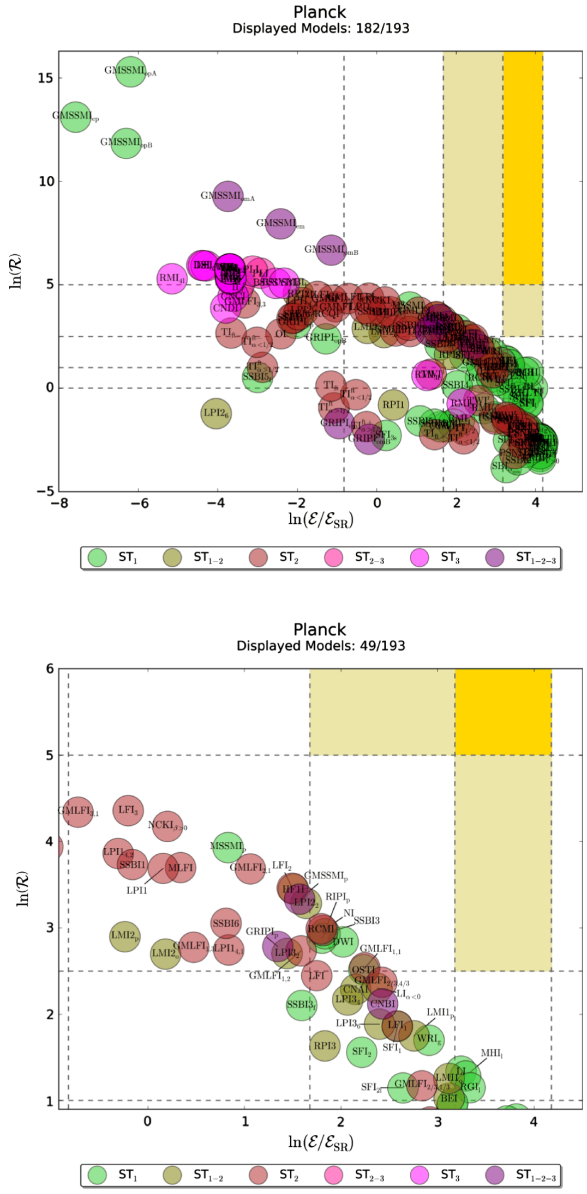

FIG. 16 (color online). Planck + BICEP2 compatibility measure, $\mathcal{R}$, versus Planck's evidences normalized to slow roll. The yellow rectangle in the top right encompasses the "strongly compatible" models that lie in the Planck-alone "inconclusive" zone (with respect to Planck's best model); the light yellow rectangles encompass the "strongly compatible" models that lie in the "weakly disfavored" zone (top left) and the "moderately compatible" models that lie in the "inconclusive" zone (bottom right). One can see that these rectangles are empty. The bottom panel is a zoom into the neighborhood of these regions. Among the models favored by Planck data alone, there are only a few for which Planck and BICEP2 data are, at most, weakly compatible [$1 < \ln(\mathcal{R}) < 2.5$].

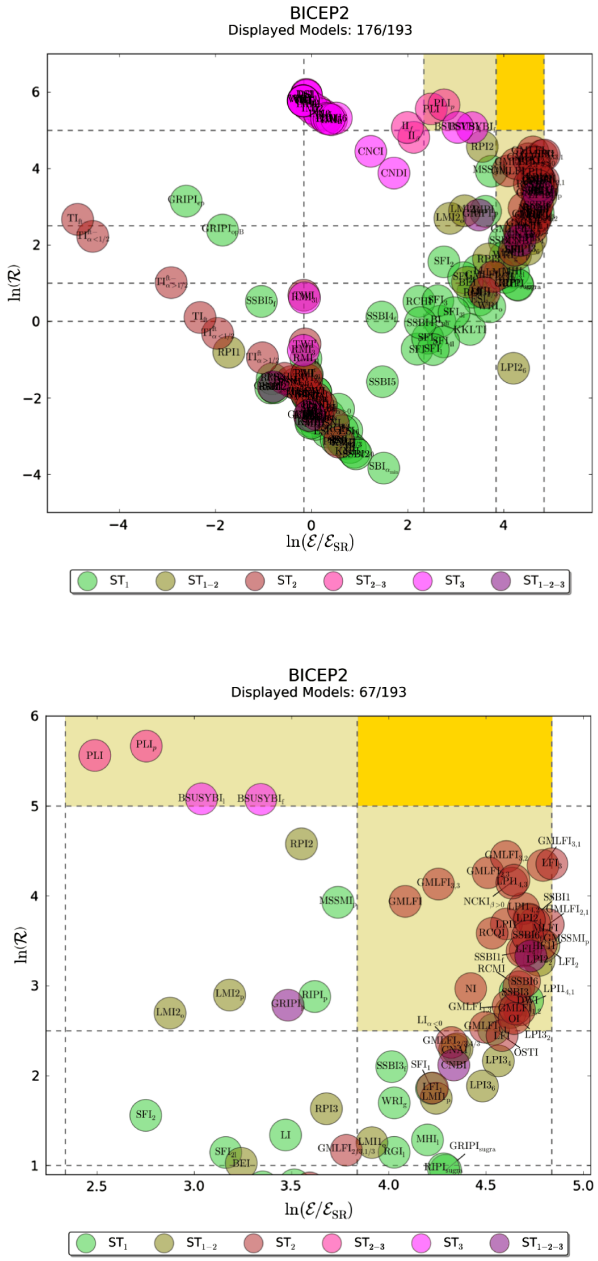

FIG. 17 (color online). Planck + BICEP2 compatibility measure, $\mathcal{R}$, versus BICEP2 evidences normalized to slow roll. The yellow rectangle in the top right encompasses the "strongly compatible" models that lie in the BICEP2-alone "inconclusive" zone (with respect to BICEP2's best model); the light yellow rectangles encompass the "strongly compatible" models that lie in the "weakly disfavored" zone (top left) and the "moderately compatible" models that lie in the "inconclusive" zone (bottom right). The bottom panel is a zoom into the neighborhood of these regions. The models favored by BICEP2 data alone are found in the region where Planck and BICEP2 are moderately compatible.

compatibility according to the Jeffreys scale (i.e. models having $0 < \ln\mathcal{R} \ll 5$). The two best models are now HF1I and $\rm LFI_2$. Then, in the inconclusive zone (with respect to the new best model) one has $\rm LPI2_2$, $\rm GMSSMI_p$, DWI, $\rm GLMFI_{2,1}$, RCMI, SSBI3, OSTI, $\rm GMLFI_{1,1}$, NI, $\rm GMLFI_{2/3,4/3}$, $\rm LI_{\alpha<0}$, $\rm NCKI_{\beta>0}$, $\rm GMLFI_{1,2}$, $\rm LFI_3$, CNBI, $\rm LPI3_4$, MLFI, CNAI, LFI, MHI, $\rm LPI3_2$, $\rm LPI3_6$, $\rm LMI1_p$, $\rm LFI_1$, and $\rm SFI_1$. It is interesting to notice that, among the previous models, none of them is in the strongly compatible

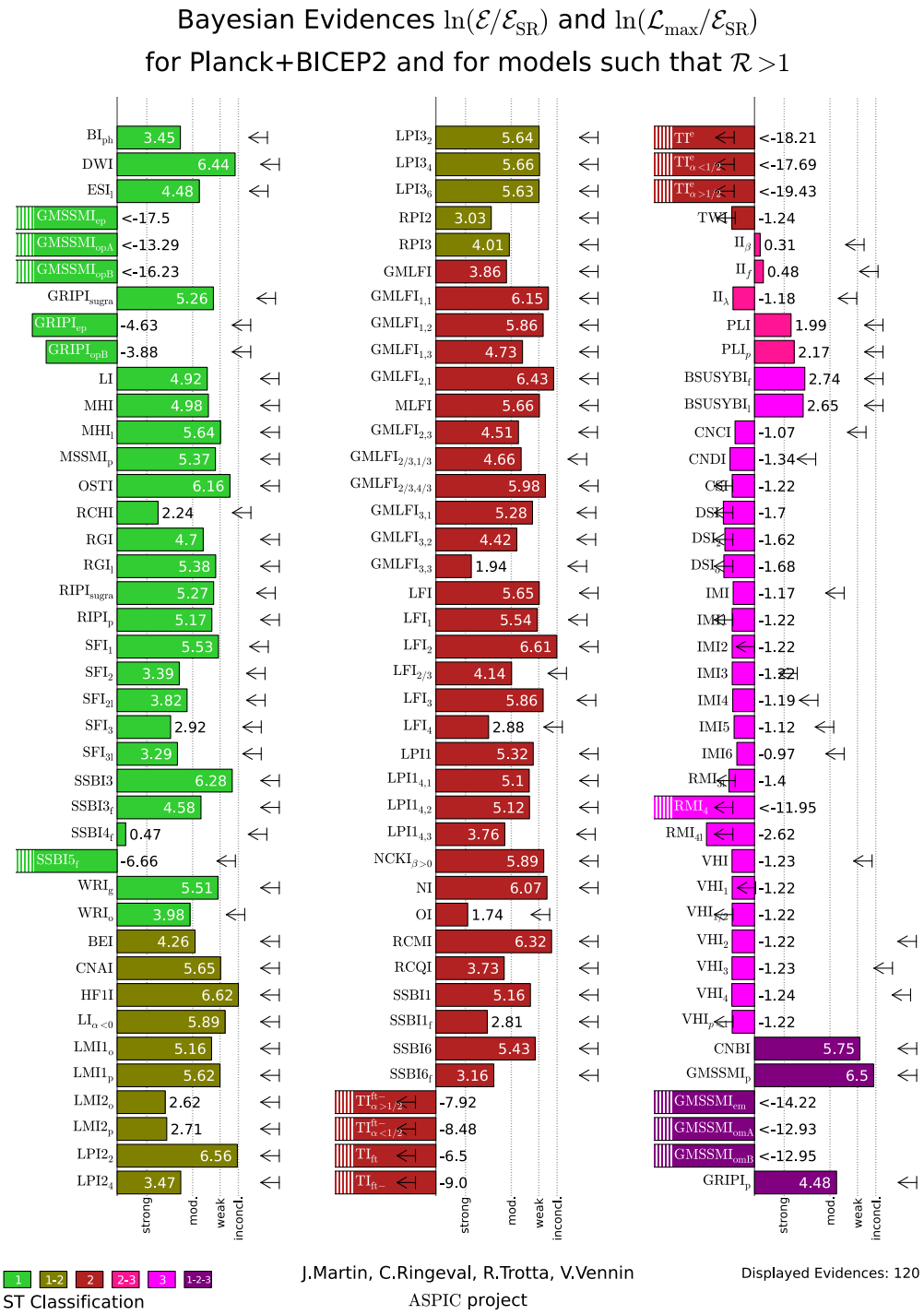

FIG. 18 (color online). Evidences (Bayes factor) and absolute upper bounds to the Bayes factors, from Planck and BICEP2 data combined, for the models such that $\mathcal{R} > 1$ only. The reference model is the same slow-roll model as in Figs. 11 and 13, and the vertical dotted lines refer to the Jeffreys scale with respect to the best model, here HF1I.

zone. This is yet another consequence of the tension between Planck and BICEP2 under an inflationary prior assumption. We also notice that all the models in the Planck + BICEP2 inconclusive zone are in the BICEP2 inconclusive zone while only one (i.e. MHI_1) is in the Planck inconclusive zone. On the other hand, the LFI_4 scenario which was in the list of inconclusive models for BICEP2 becomes moderately disfavored when adding Planck.

V. CONCLUSIONS

Let us now summarize our main conclusions. If the BICEP2 data stand the test of time and are confirmed as a

signature of tensor modes of inflationary origin, they do represent a major advance in our understanding of inflation and primordial cosmology. Indeed, for the first time, we would now have a measurement of the energy scale of inflation: the GUT scale. Other important consequences were also discussed in the Introduction.

The main issue addressed in the present article was the compatibility of the Planck data with the BICEP2 data assuming an inflationary prior. Several indicators have been used to quantify the tension between these two measurements. First, assuming slow roll, we have shown that our posterior odds measure of compatibility gives $\mathcal{R}_{\rm SR} \simeq 1$. This means that we are not in a position to establish that Planck and BICEP2 are compatible at a statistically significant level assuming a slow-roll model. But, clearly, we cannot either prove that the two data sets are incompatible (again, assuming slow roll): we are precisely in a regime where one cannot conclude. Second, we have also computed the $\mathcal{R}$ factor for all the *Encyclopædia Inflationaris* scenarios and shown that the undecided situation just described is changed. We have found that the zone of strongly compatible models contain no "good" Planck or BICEP2 models (i.e. "good" models are defined to be models in the inconclusive zone with respect to the best models of each data set alone). Moreover, all the models for which we can be sure that Planck and BICEP2 are compatible ($\ln\mathcal{R} > 5$) are either strongly or moderately disfavored by Planck (except three models that are only weakly disfavored, i.e. $\mathrm{BSUSYBI}_1$, $\mathrm{GMSSMI}_{\mathrm{omB}}$, and $\mathrm{GMSSMI}_{\mathrm{em}}$). Third, for models such that $\mathcal{R} > 1$, we have derived the updated value of the Bayesian evidence. We have found that, for all the best Planck + BICEP2 models (those which are in the inconclusive zone with respect to the best Planck + BICEP2 model LFI_3), we have $1 < \ln\mathcal{R} < 5$; i.e. for none of them Planck and BICEP2 appear compatible at a strong evidence level. Fourth, as was established in Ref. [25], the Planck data favor category 1 models, namely models with a potential having a plateau shape (the best model was KMIII but the inconclusive zone contained other scenarios, for instance the Starobinsky model). However, these models are disfavored by the BICEP2 data for which the best model is LFI_3 (a category 2 model) and have $\mathcal{R}$ factors less than unity. Therefore, we face a situation where Planck and BICEP2 are not strongly compatible. Moreover, as discussed above, several hints all indicate that the two measurements could in fact be incompatible although, in the present situation, it is too early to make a final judgment.

Another important message of this work is that, assuming BICEP2 alone or Planck + BICEP2 when possible (i.e. for $\ln\mathcal{R} > 1$) does not single out a particular model, for instance $m^2\phi^2$. From a theoretical point of view, $m^2\phi^2$ may seem *a priori* quite attractive. However, given either BICEP2 or Planck + BICEP2, it is not the only winner, and other types of models are still performing as well as this simple potential. As a consequence, in the present situation, it seems meaningless to focus the model building efforts only on large field models.

In view of our result, the most important next step is to confirm that the B-mode polarization detection by BICEP2 is truly of primordial origin. Hopefully, this will help to resolve the tension between the two data sets and thus their incompatibility for the Planck best scenarios.

Once done, if the detection of a nonvanishing r is confirmed, one will have to measure the tensor spectral index $n_{\rm T}$. The sign of $n_{\rm T}$ already carries very important information and has the potential to confirm or exclude different challengers to inflation. Indeed, inflation generically predicts a red spectrum, namely $n_{\rm T} < 0$; see Eq. (24). If one finds a blue spectrum $n_{\rm T} > 0$, this would certainly be difficult (and/or contrived) to explain in this framework and alternatives such as, for instance, string gas cosmology [147], which predicts a blue spectrum, would be a natural solution.

For a red spectrum, the next-to-next pressing question will be to verify the simplest consistency relation of Eq. (28), namely [148,149]

$$\frac{r}{n_{\rm T}} \simeq -8, \tag{34}$$

which is independent of the shape of the potential (but not of the inflationary classes of models).

Only after these three steps have been completed, would one be in a position to claim that inflation has been really seen in the sky. It should be clear from the above considerations that this is not yet the case.

ACKNOWLEDGMENTS

This work is partially supported by the ESA Belgian Federal PRODEX Grant No. 4000103071 and the Wallonia-Brussels Federation Grant ARC No. 11/15-040.

Note added.—On the same day this paper was made public, Ref. [150] appeared and suggested that B modes emission by polarized dust foregrounds could have been underestimated in the BICEP2 measurements. If confirmed, such a contribution from foregrounds could indeed help to alleviate the tension reported here between Planck and BICEP2 for various inflationary models.

APPENDIX: BAYESIAN COMPATIBILITY BETWEEN DATA SETS

In this section we illustrate how the $\mathcal{R}$ factor measures the degree of compatibility/incompatibility between two data sets given a model $\mathcal{M}$.

1. Toy example

We consider a toy model $\mathcal{M}$ described by a single parameter θ, the prior of which is uniform in the interval $[\alpha,\beta]$ and has a density $V_\pi^{-1} \equiv (\beta-\alpha)^{-1}$. Let us evaluate $\mathcal{R}$ associated with two data sets $D_{\rm A}$ and $D_{\rm B}$ in various idealized cases as sketched in Fig. 19. Their respective likelihoods are assumed to be Heaviside functions having a maximum value $\mathcal{L}_i^{\max}$ over a support $\delta\theta_i$ (i being A or B). For "case 1" represented in Fig. 19, one gets

$$\mathcal{R} = \frac{\int \mathcal{L}_{\rm A}(\theta)\mathcal{L}_{\rm B}(\theta)\pi(\theta){\rm d}\theta}{\int \mathcal{L}_{\rm A}(\theta)\pi(\theta){\rm d}\theta \int \mathcal{L}_{\rm B}(\theta)\pi(\theta){\rm d}\theta} = \frac{V_\pi \delta\theta_{\rm AB}}{\delta\theta_{\rm A}\delta\theta_{\rm B}}$$
$$= \frac{\delta\theta_{\rm AB}}{\min(\delta\theta_{\rm A},\delta\theta_{\rm B})} \times \frac{1}{\max(\delta\theta_{\rm A},\delta\theta_{\rm B})/V_\pi}. \qquad \text{(A1)}$$

The quantity $\delta\theta_{\rm AB}$ stands for the overlapping range of θ values between the two likelihoods. We point out that the maximum likelihood values cancel out and have no influence on $\mathcal{R}$. In the second line of Eq. (A1), we have highlighted a first factor which is always less than unity since $\delta\theta_{\rm AB} \leq \min(\delta\theta_{\rm A},\delta\theta_{\rm B})$. The second term is the inverse of the factor by which the prior volume has been reduced by the less constraining data set. Provided the less constraining data set (i.e. the one with the largest support of the likelihood) remains informative, namely $\max(\delta\theta_{\rm A},\delta\theta_{\rm B}) < V_\pi$, this second term in Eq. (A1) is always greater than unity. As expected for a Bayesian quantity, $\mathcal{R}$ measures how much the likelihoods of the two data sets overlap balanced by how much information has been gained with respect to the initial prior volume. For instance, "case 2" in Fig. 19 yields $\delta\theta_{\rm AB} = \min(\delta\theta_{\rm A},\delta\theta_{\rm B}) = \delta\theta_{\rm B}$ and $\mathcal{R} = V_\pi/\delta\theta_{\rm A} > 1$, so long as $D_{\rm A}$ is informative ($\delta\theta_{\rm A} < V_\pi$). Notice that one would get exactly the same result for $\delta\theta_{\rm AB} = \delta\theta_{\rm A} = \delta\theta_{\rm B}$. "Case 4" represents a situation in which the worse data set, here $D_{\rm A}$, becomes uninformative as the likelihood support encompasses the whole prior volume ($\delta\theta_{\rm A} = V_\pi$) and $\mathcal{R} = 1$. In other words, even though the likelihoods perfectly overlap, $\mathcal{R} = 1$ indicates that one cannot conclude on the compatibility of the two data sets precisely because one of them is uninformative. Finally, "case 3" is the worse case scenario $\delta\theta_{\rm AB} = 0$ and $\mathcal{R} = 0$ signaling a complete incompatibility between $D_{\rm A}$ and $D_{\rm B}$ under the model $\mathcal{M}$.

In view of the marginalized distributions represented in Fig. 3, the posterior of ϵ_1 exhibits a situation typical of case 1. For all the other parameters, the BICEP2 posteriors are always encompassing those associated with Planck,

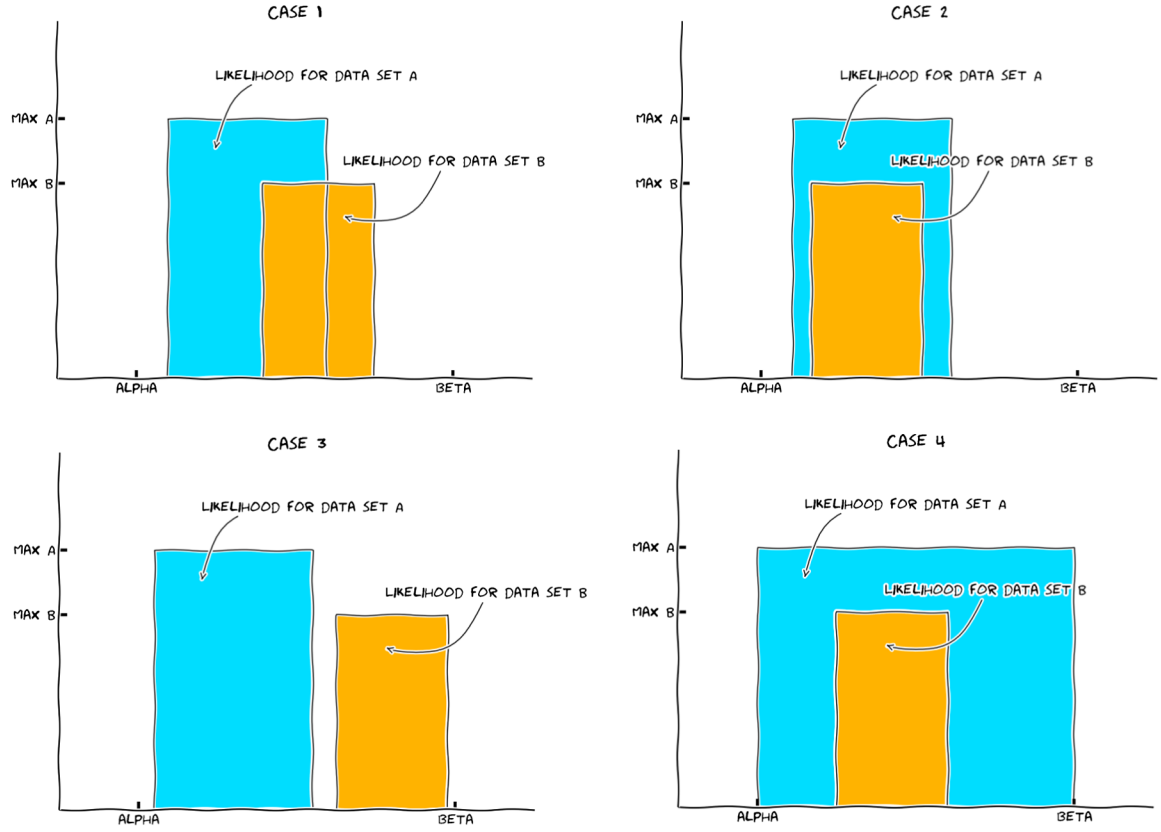

FIG. 19 (color online). Four prototypical situations when combining two data sets $D_{\rm A}$ and $D_{\rm B}$. Their respective likelihoods may overlap, or not, within the prior volume, or not. As seen in Fig. 3, Planck and BICEP2 under the slow-roll model prior (SR) could be idealized as "case 2" for the cosmological parameters which ends up being constrained by BICEP2 alone ($\mathcal{R} > 1$), as "case 4" for those not constrained at all ($\mathcal{R} = 1$) and as "case 1" over the ϵ_1 direction ($\mathcal{R} < 1$).

some being informative and others uninformative. Therefore, some directions in the parameter space are typical of case 4 (as for instance ϵ_2 and ϵ_3) while others are typical of case 2 (as for instance $\theta_{\rm MC}$ and P_*). As a result, one may expect the $\mathcal{R}_{\rm SR}$ factor between Planck and BICEP2 for the model $\mathcal{M} = {\rm SR}$ to be pushed toward unity by all the uninformative posteriors from BICEP2, less than unity by the ϵ_1 posterior and more than unity by the compatible posteriors, a situation more complex than what is advocated in Ref. [136]. In the following, we provide a semianalytic calculation confirming the numerical calculation of Sec. III C and showing that those effects roughly compensate to give $\mathcal{R}_{\rm SR}$ close to unity.

2. Semianalytic approach

In the following, we split the cosmological, astrophysical, and instrumental parameters associated with the Planck likelihood into two sets $\theta_{\rm s} = (\theta_{\rm lcdm}, \theta_{\rm n})$ with

$$\begin{aligned}\theta_{\rm lcdm} &\equiv (\Omega_{\rm b}h^2, \Omega_{\rm c}h^2, \tau, 100\theta_{\rm MC}),\\ \theta_{\rm n} &\equiv (A_{100}^{\rm PS}, A_{143}^{\rm PS}, A_{217}^{\rm PS}, r_{143\times217}^{\rm PS}, A_{143}^{\rm CIB}, A_{217}^{\rm CIB}, r_{143\times217}^{\rm CIB},\\ &\quad\times\gamma^{\rm CIB}, A_{\rm tSZ}, A_{\rm kSZ}, \xi^{\rm tSZ\times CIB}, c_{100}, c_{217}, \beta_1^1),\end{aligned} \tag{A2}$$

noticing that the BICEP2 likelihood only involves the $\theta_{\rm lcdm}$ set. In order to simplify notation we denote by ε the set of primordial parameters $\ln(10^{10}P_*)$, $\log(\epsilon_1)$, ϵ_2, and ϵ_3 and by $D_{\rm p}$ and $D_{\rm b}$ the Planck and BICEP2 data sets. From the definition of $\mathcal{R}_{\rm SR}$ one has

$$\begin{aligned}\mathcal{R}_{\rm SR} &= \frac{\mathcal{E}(D_{\rm p}, D_{\rm b}|{\rm SR})}{\mathcal{E}(D_{\rm p}|{\rm SR})\mathcal{E}(D_{\rm b}|{\rm SR})}\\ &= \mathcal{R}_{\rm REF}\frac{\frac{\mathcal{E}(D_{\rm p},D_{\rm b}|{\rm SR})}{\mathcal{E}(D_{\rm p},D_{\rm b}|\mathcal{M}_{\rm REF})}}{\frac{\mathcal{E}(D_{\rm p}|{\rm SR})}{\mathcal{E}(D_{\rm p}|\mathcal{M}_{\rm REF})}\frac{\mathcal{E}(D_{\rm b}|{\rm SR})}{\mathcal{E}(D_{\rm b}|\mathcal{M}_{\rm REF})}}.\end{aligned} \tag{A3}$$

Here we have introduced a reference model $\mathcal{M}_{\rm REF}$ such that the last term in the above equation is a ratio of Bayes factors that can be computed quickly from the effective likelihood method discussed in Sec. II. The difficulty has been moved into estimating $\mathcal{R}_{\rm REF}$, i.e. the compatibility factor between Planck and BICEP2 under some reference model. However, the arbitrariness in choosing $\mathcal{M}_{\rm REF}$ allows us to define it with a very convenient prior, namely

$$\pi(\varepsilon) = \delta(\varepsilon - \varepsilon_{\rm f}), \tag{A4}$$

where $\varepsilon_{\rm f}$ are some fixed values of the primordial parameters. The evidence of $\mathcal{M}_{\rm REF}$ using Planck data alone is given by

$$\mathcal{E}(D_{\rm p}|\mathcal{M}_{\rm REF}) = \int \bar{\mathcal{L}}_{\rm p}(\varepsilon_{\rm f}, \theta_{\rm lcdm})\pi(\theta_{\rm lcdm}){\rm d}\theta_{\rm lcdm}, \tag{A5}$$

where we have defined

$$\bar{\mathcal{L}}_{\rm p}(\varepsilon_{\rm f}, \theta_{\rm lcdm}) \equiv \int \mathcal{L}_{\rm p}(\varepsilon_{\rm f}, \theta_{\rm lcdm}, \theta_{\rm n})\pi(\theta_{\rm n}){\rm d}\theta_{\rm n}. \tag{A6}$$

Similarly, for Planck and BICEP2 data combined, one has

$$\begin{aligned}\mathcal{E}(D_{\rm p}, D_{\rm b}|\mathcal{M}_{\rm REF}) = \int &\bar{\mathcal{L}}_{\rm p}(\varepsilon_{\rm f}, \theta_{\rm lcdm})\mathcal{L}_{\rm b}(\varepsilon_{\rm f}, \theta_{\rm lcdm})\\ &\times\pi(\theta_{\rm lcdm}){\rm d}\theta_{\rm lcdm},\end{aligned} \tag{A7}$$

and for the BICEP2 data alone the evidence reads

$$\mathcal{E}(D_{\rm b}|\mathcal{M}_{\rm REF}) = \int \mathcal{L}_{\rm b}(\varepsilon_{\rm f}, \theta_{\rm lcdm})\pi(\theta_{\rm lcdm}){\rm d}\theta_{\rm lcdm}. \tag{A8}$$

These expressions are exact, and we now make some approximations. From the posteriors of Fig. 3, one sees that, over all the cosmological parameters $\theta_{\rm lcdm}$, the marginalized Planck likelihood $\bar{\mathcal{L}}_{\rm p}(\varepsilon_{\rm f}, \theta_{\rm lcdm})$ is strongly peaked inside the support of $\mathcal{L}_{\rm b}(\varepsilon_{\rm f}, \theta_{\rm lcdm})$. Therefore, Eq. (A7) can be approximated by

$$\begin{aligned}\mathcal{E}(D_{\rm p}, D_{\rm b}|\mathcal{M}_{\rm REF}) \simeq &\mathcal{L}_{\rm b}(\varepsilon_{\rm f}, \theta_{\rm lcdm}^{\rm max})\\ &\times\int \bar{\mathcal{L}}_{\rm p}(\varepsilon_{\rm f}, \theta_{\rm lcdm})\pi(\theta_{\rm lcdm}){\rm d}\theta_{\rm lcdm},\end{aligned} \tag{A9}$$

where $\theta_{\rm lcdm}^{\rm max}$ are the cosmological parameters at which $\bar{\mathcal{L}}_{\rm p}$ is maximal given $\varepsilon_{\rm f}$. From this expression, together with Eqs. (A5) and (A8), one gets

$$\mathcal{R}_{\rm REF} \simeq \frac{\mathcal{L}_{\rm b}(\varepsilon_{\rm f}, \theta_{\rm lcdm}^{\rm max})}{\int \mathcal{L}_{\rm b}(\varepsilon_{\rm f}, \theta_{\rm lcdm})\pi(\theta_{\rm lcdm}){\rm d}\theta_{\rm lcdm}}, \tag{A10}$$

which, apart from the location $\theta_{\rm lcdm}^{\rm max}$, depends on the BICEP2 likelihood only. The evidence appearing in the denominator is a four-dimensional integral over $\theta_{\rm lcdm}$ (or five-dimensional if one marginalizes over ϵ_3), as opposed to a 19-dimensional integral for the bare Planck likelihood. In practice, we have chosen $\varepsilon_{\rm f}$ as the primordial parameters associated with the best fit model of Planck and BICEP2 combined and have evaluated Eq. (A10) using the MULTINEST algorithm [134,135]. This method yields

$$\ln(\mathcal{R}_{\rm SR}) \simeq -0.01 \pm 0.3, \tag{A11}$$

where the quoted interval is a systematic error estimated by performing various nested integrations having a number of live points between 500 and 1000. This value is compatible with the full numerical integration presented in Sec. III C.

[1] P. Ade *et al.* (BICEP2 Collaboration), Phys. Rev. Lett. **112**, 241101 (2014).
[2] H. Liu, P. Mertsch, and S. Sarkar, Astrophys. J. **789**, L29 (2014).
[3] S. Saga, M. Shiraishi, and K. Ichiki, arXiv:1405.4810.
[4] C. Ringeval, T. Boehm, and R. Durrer, arXiv:hep-th/0307100.
[5] A. Moss and L. Pogosian, Phys. Rev. Lett. **112**, 171302 (2014).
[6] J. Lizarraga, J. Urrestilla, D. Daverio, M. Hindmarsh, M. Kunz, and A. R. Liddle, Phys. Rev. Lett. **112**, 171301 (2014).
[7] R. Durrer, D. G. Figueroa, and M. Kunz, arXiv:1404.3855.
[8] C. Bonvin, R. Durrer, and R. Maartens, Phys. Rev. Lett. **112**, 191303 (2014).
[9] C. Ringeval, Adv. Astron. **2010**, 380507 (2010).
[10] P. Ade *et al.* (Planck Collaboration), arXiv:1303.5085.
[11] L. P. Grishchuk, Sov. Phys. JETP **40**, 409 (1975).
[12] L. P. Grishchuk, Nuovo Cimento Lett. **12**, 60 (1975).
[13] M. J. Mortonson and U. Seljak, arXiv:1405.5857.
[14] P. Ade *et al.* (Planck Collaboration), arXiv:1405.0871.
[15] A. A. Starobinsky, Phys. Lett. **91B**, 99 (1980).
[16] A. H. Guth, Phys. Rev. D **23**, 347 (1981).
[17] A. D. Linde, Phys. Lett. **108B**, 389 (1982).
[18] A. A. Starobinsky, Phys. Lett. **117B**, 175 (1982).
[19] A. H. Guth and S. Y. Pi, Phys. Rev. Lett. **49**, 1110 (1982).
[20] A. Albrecht and P. J. Steinhardt, Phys. Rev. Lett. **48**, 1220 (1982).
[21] J. M. Bardeen, P. J. Steinhardt, and M. S. Turner, Phys. Rev. D **28**, 679 (1983).
[22] A. D. Linde, JETP Lett. **38**, 176 (1983).
[23] V. F. Mukhanov and G. V. Chibisov, JETP Lett. **33**, 532 (1981).
[24] C. M. Ho and S. D. H. Hsu, J. High Energy Phys. 07 (2014) 060.
[25] J. Martin, C. Ringeval, R. Trotta, and V. Vennin, J. Cosmol. Astropart. Phys. 03 (2014) 039.
[26] T. Kobayashi, M. Yamaguchi, and J. Yokoyama, Phys. Rev. Lett. **105**, 231302 (2010).
[27] T. Kobayashi, M. Yamaguchi, and J. Yokoyama, Phys. Rev. D **83**, 103524 (2011).
[28] C. Armendariz-Picon, T. Damour, and V. F. Mukhanov, Phys. Lett. B **458**, 209 (1999).
[29] J. Garriga and V. F. Mukhanov, Phys. Lett. B **458**, 219 (1999).
[30] D. Wands, Lect. Notes Phys. **738**, 275 (2008).
[31] A. R. Liddle, A. Mazumdar, and F. E. Schunck, Phys. Rev. D **58**, 061301 (1998).
[32] S. A. Kim and A. R. Liddle, Phys. Rev. D **74**, 023513 (2006).
[33] Y.-S. Piao, Phys. Rev. D **74**, 047302 (2006).
[34] R. Easther, J. Frazer, H. V. Peiris, and L. C. Price, Phys. Rev. Lett. **112**, 161302 (2014).
[35] S. Dimopoulos, S. Kachru, J. McGreevy, and J. G. Wacker, J. Cosmol. Astropart. Phys. 08 (2008) 003.
[36] J. M. Maldacena, J. High Energy Phys. 05 (2003) 013.
[37] P. Ade *et al.* (Planck Collaboration), arXiv:1303.5076 [Astron. Astrophys. (to be published)].
[38] P. Ade *et al.* (Planck Collaboration), arXiv:1303.5082.
[39] A. A. Starobinsky, Lect. Notes Phys. **246**, 107 (1986).
[40] A. A. Starobinsky and J. Yokoyama, Phys. Rev. D **50**, 6357 (1994).
[41] J. Martin and M. Musso, Phys. Rev. D **73**, 043516 (2006).
[42] W. H. Kinney and K. Freese, arXiv:1404.4614.
[43] A. D. Linde, Mod. Phys. Lett. A **01**, 81 (1986).
[44] A. D. Linde, Phys. Lett. B **175**, 395 (1986).
[45] A. Goncharov, A. D. Linde, and V. F. Mukhanov, Int. J. Mod. Phys. A **02**, 561 (1987).
[46] D. H. Lyth, Phys. Rev. Lett. **78**, 1861 (1997).
[47] S. Antusch and D. Nolde, J. Cosmol. Astropart. Phys. 05 (2014) 035.
[48] D. Baumann and L. McAllister, arXiv:1404.2601.
[49] J. Martin, C.R. Phys. **13**, 566 (2012).
[50] M. S. Turner and L. M. Widrow, Phys. Rev. D **37**, 2743 (1988).
[51] B. Ratra, Astrophys. J. **391**, L1 (1992).
[52] J. Martin and J. Yokoyama, J. Cosmol. Astropart. Phys. 01 (2008) 025.
[53] W. Essey, S. Ando, and A. Kusenko, Astropart. Phys. **35**, 135 (2011).
[54] K. Dolag, M. Kachelriess, S. Ostapchenko, and R. Tomas, Astrophys. J. **727**, L4 (2011).
[55] A. Neronov and I. Vovk, Science **328**, 73 (2010).
[56] F. Tavecchio, G. Ghisellini, L. Foschini, G. Bonnoli, G. Ghirlanda, and P. Coppi, Mon. Not. R. Astron. Soc. **406**, L70 (2010).
[57] V. Demozzi, V. Mukhanov, and H. Rubinstein, J. Cosmol. Astropart. Phys. 08 (2009) 025.
[58] R. J. Ferreira, R. K. Jain, and M. S. Sloth, J. Cosmol. Astropart. Phys. 10 (2013) 004.
[59] R. J. Z. Ferreira, R. K. Jain, and M. S. Sloth, J. Cosmol. Astropart. Phys. 06 (2014) 053.
[60] V. Demozzi and C. Ringeval, J. Cosmol. Astropart. Phys. 05 (2012) 009.
[61] C. Ringeval, T. Suyama, and J. Yokoyama, J. Cosmol. Astropart. Phys. 09 (2013) 020.
[62] T. Accadia *et al.*, Nuovo Cimento Soc. Ital. Fis. C **034**, 189 (2011).
[63] P. Amaro-Seoane *et al.*, GW Notes **6**, 4 (2013).
[64] S. Kawamura *et al.*, Classical Quantum Gravity **28**, 094011 (2011).
[65] M. Ando *et al.*, Classical Quantum Gravity **27**, 084010 (2010).
[66] J. Crowder and N. J. Cornish, Phys. Rev. D **72**, 083005 (2005).
[67] K. Nakayama, S. Saito, Y. Suwa, and J. Yokoyama, J. Cosmol. Astropart. Phys. 06 (2008) 020.
[68] S. Kuroyanagi, C. Ringeval, and T. Takahashi, Phys. Rev. D **87**, 083502 (2013).
[69] L. M. Krauss and F. Wilczek, Phys. Rev. D **89**, 047501 (2014).
[70] A. Ashoorioon, P. B. Dev, and A. Mazumdar, arXiv:1211.4678.
[71] T. Markkanen, S. Rasanen, and P. Wahlman, arXiv:1407.4691.
[72] V. F. Mukhanov, H. Feldman, and R. H. Brandenberger, Phys. Rep. **215**, 203 (1992).
[73] J. Martin, Lect. Notes Phys. **669**, 199 (2005).
[74] J. Martin, Lect. Notes Phys. **738**, 193 (2008).
[75] J. M. Bardeen, Phys. Rev. D **22**, 1882 (1980).

[76] K. A. Malik and D. Wands, Phys. Rep. **475**, 1 (2009).
[77] A. Riotto, arXiv:hep-ph/0210162.
[78] L. P. Grishchuk and Y. V. Sidorov, Phys. Rev. D **42**, 3413 (1990).
[79] J. Lesgourgues, D. Polarski, and A. A. Starobinsky, Nucl. Phys. **B497**, 479 (1997).
[80] C. P. Burgess, R. Holman, and D. Hoover, Phys. Rev. D **77**, 063534 (2008).
[81] C. Kiefer and D. Polarski, Adv. Sci. Lett. **2**, 164 (2009).
[82] D. Sudarsky, Int. J. Mod. Phys. D **20**, 509 (2011).
[83] N. Pinto-Neto, G. Santos, and W. Struyve, Phys. Rev. D **85**, 083506 (2012).
[84] J. Martin, V. Vennin, and P. Peter, Phys. Rev. D **86**, 103524 (2012).
[85] S. Das, K. Lochan, S. Sahu, and T. Singh, Phys. Rev. D **88**, 085020 (2013).
[86] S. Das, S. Sahu, S. Banerjee, and T. Singh, arXiv:1404.5740.
[87] S. Galli, K. Benabed, F. Bouchet, J.-F. Cardoso, F. Elsner, E. Hivon, A. Mangilli, S. Prunet, and B. Wandelt, arXiv:1403.5271.
[88] A. Lue, L.-M. Wang, and M. Kamionkowski, Phys. Rev. Lett. **83**, 1506 (1999).
[89] S. Alexander and J. Martin, Phys. Rev. D **71**, 063526 (2005).
[90] C. R. Contaldi, J. Magueijo, and L. Smolin, Phys. Rev. Lett. **101**, 141101 (2008).
[91] J. Martin, C. Ringeval, and V. Vennin, Phys. Dark Univ., doi:10.1016/j.dark.2014.01.003 (2014).
[92] J. Martin, arXiv:1312.3720.
[93] S. Dorn, E. Ramirez, K. E. Kunze, S. Hofmann, and T. A. Enlin, J. Cosmol. Astropart. Phys. 06 (2014) 048.
[94] R. Trotta, Mon. Not. R. Astron. Soc. **378**, 72 (2007).
[95] R. Trotta, Contemp. Phys. **49**, 71 (2008).
[96] M. Hobson, S. Bridle, and O. Lahav, Mon. Not. R. Astron. Soc. **335**, 377 (2002).
[97] P. Marshall, N. Rajguru, and A. Slosar, Phys. Rev. D **73**, 067302 (2006).
[98] F. Feroz, B. C. Allanach, M. Hobson, S. S. AbdusSalam, R. Trotta, and A. M. Weber, J. High Energy Phys. 10 (2008) 064.
[99] M. E. Cabrera, J. A. Casas, R. Ruiz de Austri, and R. Trotta, Phys. Rev. D **84**, 015006 (2011).
[100] F. Feroz, K. Cranmer, M. Hobson, R. Ruiz de Austri, and R. Trotta, J. High Energy Phys. 06 (2011) 042.
[101] C. Arina, Phys. Rev. D **86**, 123527 (2012).
[102] C. Arina, arXiv:1310.5718.
[103] M. Kunz, R. Trotta, and D. Parkinson, Phys. Rev. D **74**, 023503 (2006).
[104] C. Arina, G. Bertone, and H. Silverwood, Phys. Rev. D **88**, 013002 (2013).
[105] P. Ade *et al.* (Planck Collaboration), arXiv:1303.5075.
[106] S. Hamimeche and A. Lewis, Phys. Rev. D **77**, 103013 (2008).
[107] H. Chiang *et al.*, Astrophys. J. **711**, 1123 (2010).
[108] P. Ade *et al.* (Planck Collaboration), arXiv:1303.5062.
[109] J. Dunkley *et al.* (WMAP Collaboration), Astrophys. J. Suppl. Ser. **180**, 306 (2009).
[110] G. Hinshaw *et al.* (WMAP Collaboration), Astrophys. J. Suppl. Ser. **208**, 19 (2013).
[111] C. Bennett *et al.* (WMAP Collaboration), Astrophys. J. Suppl. Ser. **208**, 20 (2013).
[112] D. Barkats *et al.* (BICEP1 Collaboration), arXiv:1310.1422.
[113] A. Lewis and S. Bridle, Phys. Rev. D **66**, 103511 (2002).
[114] A. Lewis, A. Challinor, and A. Lasenby, Astrophys. J. **538**, 473 (2000).
[115] M. S. Turner, Phys. Rev. D **28**, 1243 (1983).
[116] J. Martin and C. Ringeval, J. Cosmol. Astropart. Phys. 08 (2006) 009.
[117] C. Ringeval, Lect. Notes Phys. **738**, 243 (2008).
[118] J. Martin and C. Ringeval, Phys. Rev. D **82**, 023511 (2010).
[119] R. Easther and H. V. Peiris, Phys. Rev. D **85**, 103533 (2012).
[120] J. Martin, C. Ringeval, and R. Trotta, Phys. Rev. D **83**, 063524 (2011).
[121] C. Ringeval, Mon. Not. R. Astron. Soc. **439**, 3253 (2014).
[122] E. D. Stewart and D. H. Lyth, Phys. Lett. B **302**, 171 (1993).
[123] J.-O. Gong and E. D. Stewart, Phys. Lett. B **510**, 1 (2001).
[124] J. Martin and D. J. Schwarz, Phys. Rev. D **67**, 083512 (2003).
[125] S. Habib, K. Heitmann, G. Jungman, and C. Molina-Paris, Phys. Rev. Lett. **89**, 281301 (2002).
[126] D. J. Schwarz, C. A. Terrero-Escalante, and A. A. Garcia, Phys. Lett. B **517**, 243 (2001).
[127] S. M. Leach, A. R. Liddle, J. Martin, and D. J. Schwarz, Phys. Rev. D **66**, 023515 (2002).
[128] R. Casadio, F. Finelli, M. Luzzi, and G. Venturi, Phys. Rev. D **71**, 043517 (2005).
[129] R. Casadio, F. Finelli, M. Luzzi, and G. Venturi, Phys. Lett. B **625**, 1 (2005).
[130] R. Casadio, F. Finelli, M. Luzzi, and G. Venturi, Phys. Rev. D **72**, 103516 (2005).
[131] L. Lorenz, J. Martin, and C. Ringeval, Phys. Rev. D **78**, 083513 (2008).
[132] J. Martin, C. Ringeval, and V. Vennin, J. Cosmol. Astropart. Phys. 06 (2013) 021.
[133] J. Beltran Jimenez, M. Musso, and C. Ringeval, Phys. Rev. D **88**, 043524 (2013).
[134] F. Feroz and M. Hobson, Mon. Not. R. Astron. Soc. **384**, 449 (2008).
[135] F. Feroz, M. Hobson, and M. Bridges, Mon. Not. R. Astron. Soc. **398**, 1601 (2009).
[136] B. Audren, D. G. Figueroa, and T. Tram, arXiv:1405.1390.
[137] R. K. Jain, P. Chingangbam, L. Sriramkumar, and T. Souradeep, Phys. Rev. D **82**, 023509 (2010).
[138] C. R. Contaldi, M. Peloso, and L. Sorbo, J. Cosmol. Astropart. Phys. 07 (2014) 014.
[139] D. K. Hazra, A. Shafieloo, G. F. Smoot, and A. A. Starobinsky, Phys. Rev. Lett. **113**, 071301 (2014).
[140] D. K. Hazra, A. Shafieloo, G. F. Smoot, and A. A. Starobinsky, J. Cosmol. Astropart. Phys. 06 (2014) 061.
[141] K. N. Abazajian, G. Aslanyan, R. Easther, and L. C. Price, arXiv:1403.5922.
[142] D. J. Schwarz and C. A. Terrero-Escalante, J. Cosmol. Astropart. Phys. 08 (2004) 003.

[143] T. Kobayashi and O. Seto, Phys. Rev. D **89**, 103524 (2014).
[144] X. Calmet and V. Sanz, arXiv:1403.5100.
[145] J. Ellis, M. A. G. Garcia, D. V. Nanopoulos, and K. A. Olive, J. Cosmol. Astropart. Phys. 05 (2014) 037.
[146] L. Kofman and A. D. Linde, J. High Energy Phys. 07 (2002) 004.
[147] R. H. Brandenberger, A. Nayeri, and S. P. Patil, arXiv:1403.4927.
[148] J. Caligiuri and A. Kosowsky, Phys. Rev. Lett. **112**, 191302 (2014).
[149] S. Dodelson, arXiv:1403.6310.
[150] R. Flauger, J. C. Hill, and D. N. Spergel, arXiv:1405.7351.